Generalized α-attractors from the hyperbolic triply-punctured sphere

Mirela Babalic, Calin Iuliu Lazaroiu

Center for Geometry and Physics, Institute for Basic Science, Pohang, Republic of Korea 37673

E-mail: mirela@ibs.re.kr, calin@ibs.re.kr

arXiv:1703.06033v1 [hep-th] 17 Mar 2017

Abstract: We study generalized α-attractor models whose rescaled scalar manifold is the triply-punctured Riemann sphere $Y(2)$ endowed with its complete hyperbolic metric. Using an explicit embedding into the end compactification, we compute solutions of the cosmological evolution equations for a few globally well-behaved scalar potentials, displaying particular trajectories with inflationary behavior. In such models, the orientation-preserving isometry group of the scalar manifold is isomorphic with the permutation group on three elements, acting on $Y(2)$ as the group of anharmonic transformations. When the scalar potential is preserved by this action, α-attractor models of this type provide a geometric description of two-field "modular invariant j-models" in terms of gravity coupled to a non-linear sigma model with topologically non-trivial target and with a finite (as opposed to discrete but infinite) group of symmetries. The relation between the two perspectives is provided by the elliptic modular function λ, viewed as a field redefinition which eliminates most of the infinite unphysical ambiguity present in the Poincaré half-plane description of such models.

Contents

1 Generalized α-attractor models **4**
- 1.1 Definition of the models 4
- 1.2 Lift to the Poincaré half-plane 5
- 1.3 The inflation region of the tangent bundle 6
- 1.4 Relation to modular-invariant cosmological models 7
- 1.5 Symmetries 8

2 The hyperbolic triply-punctured sphere **9**
- 2.1 The modular curve $Y(2)$ 9
- 2.2 The end compactification 10
- 2.3 The conformal compactification 10
- 2.4 The hyperbolic metric 10
- 2.5 Uniformization to the Poincaré half-plane 11
- 2.6 Presentation of $Y(2)$ as a branched cover of the complex plane 15
- 2.7 Quotients of $Y(2)$ by $\mathfrak{B}$ 16
- 2.8 The orbifold hyperbolic metric induced on $\mathfrak{M}$ 16
- 2.9 Description of modular-invariant j-models as lifts of generalized α-attractor models 17
- 2.10 A multivalued inverse of λ 17
- 2.11 Fundamental polygons 17
- 2.12 Local holomorphic cusp coordinates on $Y(2)$ 18

3 Cosmological trajectories **20**
- 3.1 Globally well-behaved scalar potentials on $Y(2)$ 20
- 3.2 Examples of cosmological trajectories 21

4 Conclusions and further directions **31**

Introduction

In [1], we introduced a wide class of two-field cosmological models known as *generalized α-attractors*. These are derived from four-dimensional gravity coupled to a non-linear sigma model whose scalar manifold Σ is a borderless, oriented and non-compact surface of finite genus, endowed with a complete metric $\mathcal{G}$ of constant negative curvature, with a scalar potential given by a smooth real-valued function Φ defined on Σ. Such cosmological models provide a wide generalization of ordinary α-attractors [2–7], having the same universal behavior as the latter when the fields undergo slow motion along approximate geodesics flowing from any of the ends of Σ toward the compact core. The role of the parameter α is played by the quantity $\frac{1}{3|K|}$, where $K < 0$ is the Gaussian curvature of $\mathcal{G}$. Equivalently, we have $\mathcal{G} = 3\alpha G$, where G is a complete hyperbolic metric on Σ, i.e. a complete metric of constant Gaussian curvature equal to -1. As explained in the present paper, generalized α-attractors can be related to modular-invariant cosmological models [8] through uniformization [9]. They allow for multipath inflation when the scalar potential or the topology of Σ are sufficiently nontrivial and have intricate cosmological dynamics already when Σ is an elementary surface [10].

In this paper, we consider the case when Σ is the triply-punctured Riemann sphere (equivalently, the doubly-punctured complex plane) endowed with its unique complete hyperbolic metric G. With respect to this metric, the three punctures of the sphere are located at infinite distance from the compact core, determining three hyperbolic cusp regions [11, 12] of infinite length but finite area. The hyperbolic area of the triply-punctured sphere is finite and equals 2π. Such a surface can be viewed as a degeneration of a hyperbolic pair of pants, in the limit when each of the cuff lengths of the latter tends to zero. When viewed as a smooth algebraic variety, the triply-punctured Riemann sphere coincides with one of the classical non-compact modular curves [13, 14], usually denoted $Y(2)$. It is uniformized by a non-Abelian surface group $\Gamma(2)$ which is freely generated by two parabolic elements, namely the principal congruence subgroup of $\mathrm{PSL}(2,\mathbb{Z})$ at level two[1]. The uniformization map from the Poincaré half-plane is given [15] by the classical elliptic modular function λ.

The end compactification of $Y(2)$ is the unit sphere S^2. The conformal compactification (which in this case is usually denoted $X(2)$) is the unit sphere endowed with its unique orientation-compatible complex structure, i.e. the Riemann sphere $\mathbb{CP}^1$. An explicit embedding of $Y(2)$ into the Riemann sphere is obtained by restricting the inverse of the stereographic projection. A smooth scalar potential defined on $Y(2)$ is globally well-behaved in the sense of [1] iff it is induced through this projection by a smooth real-valued map $\hat{\Phi}$ defined on the sphere. Using these observations, one can describe globally well-behaved scalar potentials defined on $Y(2)$ by expanding $\hat{\Phi}$ into spherical harmonics.

As explained in [1], cosmological trajectories of the generalized α-attractor model defined by $Y(2)$ can be obtained by first computing trajectories of an appropriately lifted model defined on the Poincaré half-plane and then projecting the latter to $Y(2)$ through the uniformization map. Using this method, we compute cosmological trajectories for a

[1] In some references, the symbol $\Gamma(2)$ is used instead to denote the principal congruence subgroup of $\mathrm{SL}(2,\mathbb{Z})$ at level two. In this paper, we only use it to denote the corresponding subgroup of $\mathrm{PSL}(2,\mathbb{Z})$.

few globally well-behaved scalar potentials. In particular, we display trajectories which have inflationary behavior for small enough times. We find that the model exhibits rich cosmological dynamics already in the absence of a scalar potential, which becomes even more complex when the scalar potential is included.

The lifts [1] of our models to the Poincaré half-plane can be viewed as modular-invariant cosmological models in the sense of [8] for the modular group $\Gamma(2)$. The description provided by the lifted model, while convenient for some purposes, contains an infinite ambiguity which signals the fact that the physically-relevant scalar field is not valued in the Poincaré half-plane but in the triply-punctured sphere $Y(2)$. The uniformization map λ can be viewed as a field redefinition which eliminates this unphysical ambiguity, thus affording easier understanding of the physics near the ends of $Y(2)$.

The orientation-preserving isometry group of the hyperbolic triply-punctured sphere is isomorphic with the permutation group on three elements, acting on $Y(2)$ as the anharmonic subgroup $\mathfrak{B}$ of $\mathrm{PSL}(2,\mathbb{C})$, which permutes the three punctures. The triply-punctured sphere can be written as a six-fold branched cover $q : Y(2) \to \mathbb{C}$ of the complex plane in such a way that the composition $q \circ \lambda$ coincides with the modular j function. The anharmonic action permutes the branches of this cover, hence the topological quotient $Y(2)/\mathfrak{B}$ can be identified with the complex plane. Since q is ramified above two points of the complex plane, the hyperbolic metric of $Y(2)$ descends to a *singular* metric on the topological quotient $\mathbb{C} = Y(2)/\mathfrak{B}$. When the scalar potential Φ is preserved by the anharmonic action, the generalized α-attractor model with scalar manifold $Y(2)$ has an S_3 symmetry and the corresponding lifted model is a "j-model" in the sense of [8], being invariant under the entire classical modular group $\mathrm{PSL}(2,\mathbb{Z})$. In that case, the field redefinition provided by the elliptic modular function λ eliminates an infinite $\Gamma(2)$-ambiguity, replacing it with a finite $\mathfrak{B} \simeq S_3$ symmetry. The latter cannot be eliminated directly within the framework of generalized α-attractor models, since taking the quotient through the anharmonic action of S_3 would lead to a singular metric on the complex plane, which is disallowed in the usual construction of non-linear sigma models.

The paper is organized as follows. Section 1 briefly recalls the definition of generalized α-attractor models and the lift of their cosmological equations of motion to the Poincaré half-plane. It also explains the interpretation of the lift as a modular-invariant cosmological model in the sense of [8]. It also explains the symmetries of such models. Section 2 discusses the end and conformal compactifications as well as the hyperbolic geometry of $Y(2)$, its symmetries and its uniformization. We also explain the difference between $Y(2)$ (which coincides with the coarse moduli space of elliptic curves with level 2 structure) and the usual coarse moduli space of elliptic curves (which equals the complex plane), of which $Y(2)$ is a branched six-fold cover. This accounts for the difference between the elliptic modular functions λ and j, which differ by composition with a rational function. We also show that modular-invariant cosmological models for the classical modular group $\mathrm{SL}(2,\mathbb{Z})$ can be described as those generalized α-attractor models with scalar manifold $Y(2)$ for which the scalar potential is invariant under the action of the anharmonic group. Section 3 discusses globally well-behaved scalar potentials on the triply-punctured sphere and presents examples of numerically-computed cosmological trajectories, while Section 4 concludes.

Notations and conventions. All manifolds considered are smooth, connected, oriented and paracompact (hence also second-countable). All homeomorphisms and diffeomorphisms considered are orientation-preserving. By definition, a Lorentzian four-manifold has "mostly plus" signature. The Poincaré half-plane is the upper half-plane with complex coordinate τ:

$$\mathbb{H} = \{\tau \in \mathbb{C} \,|\, \mathrm{Im}\tau > 0\} \quad , \tag{0.1}$$

endowed with its unique complete metric of Gaussian curvature -1, which is given by:

$$\mathrm{d}s^2_{\mathbb{H}} = \frac{1}{(\mathrm{Im}\tau)^2}|\mathrm{d}\tau|^2 \quad .$$

The real coordinates on $\mathbb{H}$ are denoted by $x \overset{\text{def.}}{=} \mathrm{Re}\tau$ and $y \overset{\text{def.}}{=} \mathrm{Im}\tau$. The complex coordinate on the hyperbolic disk is denoted by u, while that on the twice-punctured complex plane is denoted by ζ. The symbol $\mathbf{i}$ denotes the imaginary unit. The *rescaled Planck mass* is defined through:

$$M_0 \overset{\text{def.}}{=} M\sqrt{\frac{2}{3}} \quad , \tag{0.2}$$

where M is the reduced Planck mass.

1 Generalized α-attractor models

In this section, we briefly recall the definition of generalized α-attractor models given in [1] and their lifts to the Poincaré half-plane. We also discuss the interpretation of this lift as a modular-invariant cosmological model in the sense of [8] and symmetries of such models.

1.1 Definition of the models

Let (Σ, G) be a non-compact oriented, connected and complete two-dimensional Riemannian manifold without boundary (the *scalar manifold*) and $\Phi : \Sigma \to \mathbb{R}$ be a smooth function (the *scalar potential*). We assume that (Σ, G) is *hyperbolic*, i.e. that G has constant Gaussian curvature equal to -1. We also assume that the fundamental group of Σ is finitely-generated. Let α be a positive constant. The rescaled metric $\mathcal{G} \overset{\text{def.}}{=} 3\alpha G$ has constant Gaussian curvature $K = -\frac{1}{3\alpha}$.

Given an oriented four-manifold X which supports Lorentzian metrics, the Einstein-Scalar theory defined by $(\Sigma, \mathcal{G}, \Phi)$ on X describes a Lorentzian metric g on X and a smooth map $\varphi : X \to \Sigma$ through the action (see [1] for the notations):

$$S[g, \varphi] = \int_X \left[\frac{M^2}{2}\mathrm{R}(g) - \frac{1}{2}\mathrm{Tr}_g\varphi^*(\mathcal{G}) - \Phi \circ \varphi\right] \mathrm{vol}_g \quad , \tag{1.1}$$

where vol_g is the volume form of (X, g), $\mathrm{R}(g)$ is the scalar curvature of g and M is the reduced Planck mass. When X is diffeomorphic with $\mathbb{R}^4$ and g is a FLRW metric with flat spatial section, solutions of the equations of motion of (1.1) for which φ depends only on the cosmological time t define *generalized α-attractor models* [1]. We shall assume that Φ is non-negative, as appropriate for cosmological applications.

Let J be the unique orientation-compatible complex structure on Σ which has the property that G is Hermitian (and hence Kähler) with respect to J. Endowing Σ with this complex structure, let ζ be a local holomorphic coordinate on Σ, defined on an open subset $\mathcal{U} \subset \Sigma$. Since G is Hermitian with respect to J, we have $\mathrm{d}s^2_G|_{\mathcal{U}} = \rho(\zeta,\bar{\zeta})^2|\mathrm{d}\zeta|^2$ for some positive function $\rho(\zeta,\bar{\zeta}) > 0$, known as the *hyperbolic density* of G with respect to ζ. Choosing a local chart $(U,(x^\mu))$ of M such that $\varphi(U) \subset \mathcal{U}$ and setting $\zeta(x) \stackrel{\text{def.}}{=} \zeta(\varphi(x))$, the map φ is described locally by the complex-valued scalar field $\zeta(x)$ and the Lagrangian density of (1.1) has the local form:

$$\mathcal{L}[g|_U,\varphi|_U] = \frac{M^2}{2}\mathrm{R}(g) - \frac{3\alpha}{2}\rho^2(\zeta,\bar{\zeta})g^{\mu\nu}\partial_\mu\zeta\partial_\nu\bar{\zeta} - \Phi(\zeta,\bar{\zeta}) \quad . \tag{1.2}$$

1.2 Lift to the Poincaré half-plane

The cosmological equations of motion of the generalized α-attractor model defined by (1.1) can be lifted [1] from Σ to the Poincaré half-plane through the J-holomorphic covering map $\pi_{\mathbb{H}} : \mathbb{H} \to \Sigma$ which uniformizes [9] (Σ, G) to $\mathbb{H}$. This presents (Σ, G) as the Riemannian quotient $\mathbb{H}/\Gamma$ (where $\Gamma \subset \mathrm{PSL}(2,\mathbb{R})$ is the uniformizing surface group [16–18]) and allows one to determine the cosmological trajectories $\varphi(t)$ by projecting solutions $\tilde{\varphi}(t) \in \mathbb{H}$ of the following equations [1, eq. (7.4)]:

$$\begin{aligned}
&\ddot{x} - \frac{2}{y}\dot{x}\dot{y} + \frac{1}{M}\sqrt{\frac{3}{2}}\left[3\alpha\frac{\dot{x}^2+\dot{y}^2}{y^2} + 2\tilde{\Phi}(x,y)\right]^{1/2}\dot{x} + \frac{1}{3\alpha}y^2\partial_x\tilde{\Phi}(x,y) = 0 \\
&\ddot{y} + \frac{1}{y}(\dot{x}^2-\dot{y}^2) + \frac{1}{M}\sqrt{\frac{3}{2}}\left[3\alpha\frac{\dot{x}^2+\dot{y}^2}{y^2} + 2\tilde{\Phi}(x,y)\right]^{1/2}\dot{y} + \frac{1}{3\alpha}y^2\partial_y\tilde{\Phi}(x,y) = 0
\end{aligned} \tag{1.3}$$

through the map $\pi_{\mathbb{H}}$. Here $\dot{} \stackrel{\text{def.}}{=} \frac{\mathrm{d}}{\mathrm{d}t}$ and $x = \mathrm{Re}\tau$, $y = \mathrm{Im}\tau$ are the Cartesian coordinates on $\mathbb{H}$ (and we wrote $\tilde{\varphi}(t) = x(t) + \mathbf{i}y(t)$), while $\tilde{\Phi} \stackrel{\text{def.}}{=} \Phi \circ \pi_{\mathbb{H}} : \mathbb{H} \to \mathbb{R}$ is the *lifted scalar potential*. As shown in [1], any cosmological trajectory $\varphi(t)$ of the generalized α-attractor model defined by (1.1) can be written as $\varphi(t) = \pi_{\mathbb{H}}(\tilde{\varphi}(t))$ for some appropriate solution $\tilde{\varphi}$ of (1.3) (which is determined by φ up to the action of Γ). In order to simplify computations, it is convenient to eliminate the Planck mass by writing (1.3) in the equivalent form:

$$\begin{aligned}
&\ddot{x} - \frac{2}{y}\dot{x}\dot{y} + \left[3\boldsymbol{\alpha}\frac{\dot{x}^2+\dot{y}^2}{y^2} + 2\tilde{\boldsymbol{\Phi}}(x,y)\right]^{1/2}\dot{x} + \frac{1}{3\boldsymbol{\alpha}}y^2\partial_x\tilde{\boldsymbol{\Phi}}(x,y) = 0 \\
&\ddot{y} + \frac{1}{y}(\dot{x}^2-\dot{y}^2) + \left[3\boldsymbol{\alpha}\frac{\dot{x}^2+\dot{y}^2}{y^2} + 2\tilde{\boldsymbol{\Phi}}(x,y)\right]^{1/2}\dot{y} + \frac{1}{3\boldsymbol{\alpha}}y^2\partial_y\tilde{\boldsymbol{\Phi}}(x,y) = 0 \quad ,
\end{aligned} \tag{1.4}$$

where $\tilde{\boldsymbol{\Phi}} \stackrel{\text{def.}}{=} \frac{\tilde{\Phi}}{M_0}$, $\boldsymbol{\alpha} \stackrel{\text{def.}}{=} \frac{\alpha}{M_0}$ and $M_0 = M\sqrt{\frac{2}{3}}$ is the rescaled Planck mass (0.2). Accordingly, the Hubble parameter can be written as $H(t) = \sqrt{M_0}\,\mathbf{H}(t)$, where (cf. [1, eq. (2.8)]):

$$\mathbf{H}(t) = \frac{1}{3}\sqrt{3\boldsymbol{\alpha}||\dot{\tilde{\varphi}}(t)||^2_{\mathbb{H}} + \tilde{\boldsymbol{\Phi}}(\tilde{\varphi}(t))} = \frac{1}{3}\sqrt{3\boldsymbol{\alpha}\frac{\dot{x}(t)^2+\dot{y}(t)^2}{y(t)^2} + \tilde{\boldsymbol{\Phi}}(x(t),y(t))} \quad ,$$

and $||.||_{\mathbb{H}}$ denotes the norm of vectors tangent to $\mathbb{H}$, computed with respect to the Poincaré metric.

1.3 The inflation region of the tangent bundle

The inflationary time periods of a trajectory $\varphi(t)$ (defined as the time intervals for which the FLRW scale factor $a(t)$ is a convex and increasing function of t) are given by the condition (cf. [1, eq. (2.12)]):

$$H(t) < H_c(\varphi(t)) \quad , \tag{1.5}$$

where:

$$H_c(p) \stackrel{\text{def.}}{=} \frac{1}{M}\sqrt{\frac{\Phi(p)}{2}}$$

is the *critical Hubble parameter* at a point $p \in \Sigma$. We have: $H_c(p) = \sqrt{M_0}\mathbf{H}_c(p)$, with $\mathbf{H}_c(p) \stackrel{\text{def.}}{=} \sqrt{\frac{\mathbf{\Phi}(p)}{3}}$, where defined $\mathbf{\Phi} \stackrel{\text{def.}}{=} \frac{1}{M_0}\Phi$. Condition (1.5) is equivalent [1] with:

$$||\dot{\varphi}(t)||^2_{\mathcal{G}} < \Phi(\varphi(t)) \quad . \tag{1.6}$$

This inequality states that a trajectory $\varphi(t)$ of the α-attractor model is inflationary for those times t for which the tangent vector $\dot{\varphi}(t) \in T_{\varphi(t)}\Sigma$ belongs to the *inflation region* defined by Φ at parameter α:

$$\mathcal{R} := \mathcal{R}_\alpha(\Phi) \stackrel{\text{def.}}{=} \{v \in T\Sigma \,|\, ||v||_G < v_c(p)\} \quad ,$$

where the *critical speed* $v_c(p) \in T_p\Sigma$ at a point p of Σ is defined through:

$$v_c(p) \stackrel{\text{def.}}{=} \sqrt{\frac{\Phi(p)}{3\alpha}} = \sqrt{\frac{\mathbf{\Phi}(p)}{3\boldsymbol{\alpha}}} \quad .$$

Notice that $\mathcal{R}$ is an open disk bundle over Σ. The quantity $v_c(p)$ gives the radius of the disk fiber of this bundle at a point $p \in \Sigma$, computed with respect to the metric G_p on $T_p\Sigma$.

Condition (1.6) can be expressed as follows in terms of any trajectory $\tilde{\varphi}$ of (1.3) which lifts φ to the Poincaré half-plane:

$$||\dot{\tilde{\varphi}}(t)||^2_{\mathbb{H}} < \frac{\tilde{\mathbf{\Phi}}(\tilde{\varphi}(t))}{3\boldsymbol{\alpha}} \text{ , i.e. } \dot{x}(t)^2 + \dot{y}(t)^2 < \frac{y^2\tilde{\mathbf{\Phi}}(x(t),y(t))}{3\boldsymbol{\alpha}} \quad . \tag{1.7}$$

For any $\tau \in \mathbb{H}$, define the *lifted critical speed* at τ on the Poincaré half-plane through:

$$\tilde{v}_c(\tau) \stackrel{\text{def.}}{=} \sqrt{\frac{\tilde{\Phi}(\tau)}{3\alpha}} = \sqrt{\frac{\tilde{\mathbf{\Phi}}(\tau)}{3\boldsymbol{\alpha}}} \quad .$$

We have $\tilde{v}_c = v_c \circ \pi_{\mathbb{H}}$, so $\tilde{v}_c$ is a Γ-invariant function defined on $\mathbb{H}$. The tangent bundle $T\mathbb{H}$ of $\mathbb{H}$ is trivial and can be identified with $\mathbb{H} \times \mathbb{R}^2$. The *lifted inflation region* defined by $\tilde{\Phi}$ at parameter α is the open subset (an open disk bundle over $\mathbb{H}$) of the total space of $T\mathbb{H}$ defined through:

$$\tilde{\mathcal{R}} := \tilde{\mathcal{R}}_\alpha(\tilde{\Phi}) \stackrel{\text{def.}}{=} \{(\tau,\tilde{v}) \in T\mathbb{H} \,|\, ||\tilde{v}||_{\mathbb{H},\tau} < \tilde{v}_c(\tau)\} \equiv \{(x,y,v) \in \mathbb{H}\times\mathbb{R}^2 \,|\, \tilde{v}_x^2+\tilde{v}_y^2 < \frac{y^2\tilde{\Phi}(x,y)}{3\alpha}\} \ ,$$

where we wrote $\tau = x+\mathbf{i}y$ and $\tilde{v} = \tilde{v}_x+\mathbf{i}\tilde{v}_y$ with real $\tilde{v}_x, \tilde{v}_y$. Notice that $\tilde{\mathcal{R}}$ is invariant under the action of Γ on $T\mathbb{H}$ and that $\mathcal{R}$ coincides with the image of $\tilde{\mathcal{R}}$ through the differential

$d\pi_{\mathbb{H}} : T\mathbb{H} \to T\Sigma$ of the uniformization map. A trajectory $\tilde{\varphi}$ of the lifted system (1.3) projects to the inflationary portion of a trajectory $\varphi = \pi_{\mathbb{H}} \circ \tilde{\varphi}$ of the α-attractor model defined by $(\Sigma, \mathcal{G})$ for those times t for which the tangent vector $\dot{\tilde{\varphi}}(t)$ belongs to $\tilde{\mathcal{R}}$. Notice that v_c has the same level sets as Φ and that $\tilde{v}_c$ has the same level sets as $\tilde{\Phi}$, though the values on the same level set generally differ.

1.4 Relation to modular-invariant cosmological models

Equations (1.3) can be viewed as the cosmological equations of motion of a "lifted" generalized α-attractor model, for which Σ is replaced by the Poincaré half-plane $\mathbb{H}$, the metric on Σ is replaced by $3\alpha G_{\mathbb{H}}$ (where $G_{\mathbb{H}}$ is the Poincaré metric of $\mathbb{H}$) and the scalar potential is replaced by the lifted potential $\tilde{\Phi}$. Notice that $\tilde{\Phi} \stackrel{\text{def.}}{=} \Phi \circ \pi_{\mathbb{H}}$ is Γ-invariant by construction and that the action of Γ on $\mathbb{H}$ is isometric (recall that Γ is a subgroup of $\mathrm{PSL}(2,\mathbb{R})$, which is the group of orientation-preserving isometries of the Poincaré half-plane). This implies that the lifted model is Γ-invariant, being of the type considered[2] in [8], up to a rescaling of the Poincaré metric by 3α (where notice that Γ need not be a subgroup of $\mathrm{PSL}(2,\mathbb{Z})$). Unlike loc. cit, however, we do *not* view this lifted model as being physical, but only as a technical tool for studying the cosmological dynamics of the original generalized α-attractor model defined by cosmological solutions of (1.1). In our approach, two distinct values of $\tilde{\varphi}$ which are related through the action of Γ are identified and they are viewed as physically equivalent; it is only the projection $\pi_{\mathbb{H}} \circ \tilde{\varphi} = \varphi$ which has a direct physical meaning. Notice that this interpretation is consistent with putative embeddings of our models into string theory. In such an embedding, Σ would be interpreted as a moduli space of internal string backgrounds, while the Poincaré half-plane would arise as a Teichmuller space of the same; the uniformizing group Γ would then arise as a group of discrete physical symmetries which identify distinct points of the Teichmuller space and hence must be quotiented out in order to correctly describe moduli field dynamics through an effective nonlinear sigma model. In such putative string theory embeddings, it would be appropriate to treat the *moduli field* φ as the physical field, rather than the "Teichmuller field" $\tilde{\varphi}$, which is only an auxiliary object without direct physical significance in the effective theory. As already shown in [10] and also illustrated later in the present paper, the effect of the projection $\pi_{\mathbb{H}}$ is quite dramatic. The uniformization map $\pi_{\mathbb{H}}$ can be viewed as an "∞ to 1" field reparameterization which eliminates an infinite unphysical ambiguity affecting the effective description of low energy[3] physics through the lifted model. In this sense, the generalized α-attractor models of [1] and the modular-invariant models of [8] are related (up to rescaling the Poincaré metric by 3α) through the uniformization map.

Suppose for definiteness that Σ has finite hyperbolic area (equivalently, that Γ is a Fuchsian group of the first kind [16, 17]), as is the case for the scalar manifold $Y(2)$ studied latter in this paper. Then Σ has only cusp ends and the limit set Λ of Γ equals the entire conformal boundary $\partial_\infty \mathbb{H} \simeq \mathrm{S}^1 \simeq \mathbb{R} \cup \{\infty\}$. This implies [16, 17] that each of the orbits of the action of Γ on the Poincaré half-plane has $\Lambda = \partial_\infty \mathbb{H}$ as its set of accumulation points.

[2] See [19, 20] for the general framework of "automorphic inflation".

[3] Low compared to the string scale.

When Φ is not constant, it follows that the lifted potential $\tilde{\Phi}$ has extremely complicated behavior near the conformal boundary. In particular, any extremum of $\tilde{\Phi}$ inside $\mathbb{H}$ is repeated a countable number of times (at all points of its Γ-orbit) and the Γ-images of any given extremum point accumulate near any point of $\partial_\infty\mathbb{H}$. The preimages through the uniformization map $\pi_{\mathbb{H}}$ of each of the cusp ideal points of Σ form a countable subset of $\partial_\infty\mathbb{H}$. As a consequence, the cosmological trajectories of the lifted model have extremely complicated behavior near the conformal boundary. Luckily, it is not these lifted trajectories (or the lifted model itself) which are of direct physical interest, but rather their projections to Σ through the uniformization map.

1.5 Symmetries

Let (Σ, G) be a geometrically-finite hyperbolic surface uniformized by the surface group $\Gamma \subset \mathrm{PSL}(2,\mathbb{R})$. The group of orientation-preserving isometries of (Σ, G) is given by:

$$\mathrm{Iso}^+(\Sigma, G) = N(\Gamma)/\Gamma \quad ,$$

where:

$$N(\Gamma) := N_{\mathrm{PSL}(2,\mathbb{R})}(\Gamma) \stackrel{\text{def.}}{=} \{A \in \mathrm{PSL}(2,\mathbb{R}) | A\Gamma A^{-1} = \Gamma\}$$

denotes the normalizer of Γ inside $\mathrm{PSL}(2,\mathbb{R})$. Since Γ is a normal subgroup of $N(\Gamma)$, we have:

$$\Sigma/\mathrm{Iso}^+(\Sigma, G) = (\mathbb{H}/\Gamma)/(N(\Gamma)/\Gamma) \simeq \mathbb{H}/N(\Gamma) \quad .$$

In the second quotient, the group $N(\Gamma)/\Gamma$ acts on Σ through:

$$a\zeta \stackrel{\text{def.}}{=} [A\tau]_\Gamma \quad \text{for} \quad a = [A]_\Gamma \in N(\Gamma)/\Gamma \quad \text{and} \quad \zeta = [\tau]_\Gamma \in \Sigma \quad , \tag{1.8}$$

where $A \in N(\Gamma)$, $\tau \in \mathbb{H}$ and $[A]_\Gamma$, $[\tau]_\Gamma$ denote the equivalence classes under the left actions of Γ on $N(\Gamma)$ and on $\mathbb{H}$. It is easy to check that the action (1.8) is well-defined.

The orientation-preserving symmetry group of the α-attractor model defined by $(\Sigma, \mathcal{G}, \Phi)$ is the subgroup of $\mathrm{Iso}^+(\Sigma, G)$ given by [1]:

$$\mathrm{Aut}^+(\Sigma, G, \Phi) = \{a \in \mathrm{Iso}^+(\Sigma, G) \,|\, \Phi(a\zeta) = \Phi(\zeta) \quad \forall \zeta \in \Sigma\} \quad .$$

This can be written as:

$$\mathrm{Aut}^+(\Sigma, G, \Phi) = [N(\Gamma) \cap \mathrm{Aut}^+(\mathbb{H}, G_{\mathbb{H}}, \tilde{\Phi})]/\Gamma \quad ,$$

where:

$$\mathrm{Aut}^+(\mathbb{H}, G_{\mathbb{H}}, \tilde{\Phi}) = \{A \in \mathrm{PSL}(2,\mathbb{R}) \,|\, \tilde{\Phi}(A\tau) = \tilde{\Phi}(\tau) \quad \forall \tau \in \mathbb{H}\}$$

is the orientation-preserving symmetry group of the lifted model, which is a subgroup of $\mathrm{PSL}(2,\mathbb{R})$. In particular, Φ is invariant under $\mathrm{Iso}^+(\Sigma, G)$ iff $\tilde{\Phi}$ is invariant under the action of $N(\Gamma)$ on $\mathbb{H}$ by fractional linear transformations. In this case, we have $\mathrm{Aut}^+(\Sigma, G, \Phi) = \mathrm{Iso}^+(\Sigma, G)$ and $N(\Gamma) \subset \mathrm{Aut}^+(\mathbb{H}, G_{\mathbb{H}}, \tilde{\Phi})$.

Remark. Suppose that $N(\Gamma)$ contains elliptic elements. Then the action of $N(\Gamma)$ on $\mathbb{H}$ and the action of $\mathrm{Iso}^+(\Sigma, G)$ on Σ have orbits whose points have non-trivial stabilizer. Due to this fact, the Poincaré metric of $\mathbb{H}$ and the hyperbolic metric G of Σ do not descend to a non-singular metric on the topological quotient $S \stackrel{\text{def.}}{=} \mathbb{H}/N(\Gamma) \simeq \Sigma/\mathrm{Iso}^+(\Sigma, G)$. Rather, they descend to an orbifold metric on the *orbifold* quotient $\mathbb{H} /\!\!/ N(\Gamma) \simeq \Sigma /\!\!/ \mathrm{Iso}^+(\Sigma, G)$, which has underlying space S. If $s_1, \ldots, s_k \in S$ denote the singular points of this orbifold quotient, then the orbifold metric can be viewed as a metric defined on $S \setminus \{s_1, \ldots, s_k\}$ which has conical singularities at each of the points $s_1, \ldots, s_k$. We will see an example of this in the next section.

2 The hyperbolic triply-punctured sphere

In this section, we discuss the geometry of the hyperbolic triply-punctured sphere $Y(2)$, its end and conformal compactifications and its uniformization to the Poincaré half-plane and to the hyperbolic disk. We also discuss the oriented isometry group of $Y(2)$ and the topological and orbifold quotients of $Y(2)$ by this group.

2.1 The modular curve $Y(2)$

The unit sphere $\mathrm{S}^2 = \{(x_1, x_2, x_3) \in \mathbb{R}^3 \,|\, x_1^2 + x_2^2 + x_3^2 = 1\}$ admits a unique [4] orientation-compatible complex structure I, which makes the complex manifold (S^2, I) biholomorphic with the Riemann sphere $\mathbb{CP}^1$. Let p_1, p_2, p_3 be any three distinct points of $\mathrm{S}^2 \simeq \mathbb{CP}^1$. By definition, a *triply punctured Riemann sphere* is the surface:

$$Y(2) \stackrel{\text{def.}}{=} \mathbb{CP}^1 \setminus \{p_1, p_2, p_3\} \quad ,$$

endowed with the complex structure $J = I|_{Y(2)}$ induced from $\mathbb{CP}^1$. This complex manifold of complex dimension one is a classical example of a non-compact modular curve. It is uniquely determined up to biholomorphism, since three distinct points of $\mathbb{CP}^1$ can be moved together in arbitrary position by acting with an element of the biholomorphism group of $\mathbb{CP}^1$, which is isomorphic with the Moebius group $\mathrm{PSL}(2, \mathbb{C})$. Up to such a transformation, one can therefore take:

$$p_1 = \nu \stackrel{\text{def.}}{=} (0, 0, 1) \quad , \quad p_2 = \sigma \stackrel{\text{def.}}{=} (0, 0, -1) \quad , \quad p_3 = p \stackrel{\text{def.}}{=} (1, 0, 0) \quad ,$$

where ν and σ are the north and south poles of S^2.

Let ψ and θ be spherical coordinates on S^2, thus:

$$x_1 = \sin\psi \cos\theta \quad , \quad x_2 = \sin\psi \sin\theta \quad , \quad x_3 = \cos\psi \quad , \tag{2.1}$$

where $\psi \in [0, \pi]$ and $\theta \in [0, 2\pi)$. Then the points ν and σ correspond respectively to $\psi = 0$ and $\psi = \pi$, while p corresponds to $\psi = \frac{\pi}{2}$ and $\theta = 0$. The stereographic projection from the north pole ν:

$$\zeta = \cot\left(\frac{\psi}{2}\right) e^{\mathbf{i}\theta} \in \mathbb{C} \tag{2.2}$$

[4] Up to orientation-preserving diffeomorphism.

is a biholomorphism from $\mathrm{S}^2 \simeq \mathbb{CP}^1 \setminus \{\nu\}$ to the complex plane $\mathbb{C}$ with complex coordinate ζ. This maps ν to the point at infinity (which is not part of $\mathbb{C}$) and σ to the origin $\zeta = 0$ of the complex plane. It maps p to the point $\zeta = 1$. As a consequence, one can identify:

$$Y(2) = \mathbb{C} \setminus \{0, 1\} \quad .$$

2.2 The end compactification

Since $Y(2)$ is a planar surface, its end (a.k.a. Kerekjarto-Stoilow [21, 22]) compactification $\widehat{Y(2)}$ coincides with the unit sphere S^2. An explicit embedding $Y(2) \hookrightarrow \mathrm{S}^2$ is given by:

$$\psi = 2\,\mathrm{arccot}(|\zeta|) \quad , \quad \theta = \arg(\zeta) \quad . \tag{2.3}$$

In particular, the punctures $p_1 = \nu \equiv \infty$, $p_2 = \sigma \equiv 0$ and $p_3 = p \equiv 1$ coincide with the ideal points of $\widehat{Y(2)}$ and hence can be identified with the ends of $Y(2)$.

2.3 The conformal compactification

Since $\widehat{Y(2)} \simeq \mathrm{S}^2$ admits a unique orientation-compatible complex structure I, the prolongation [1, 23, 24] of the complex structure J of $Y(2)$ coincides with I. Hence the conformal compactification [1] of $Y(2)$ coincides with $(\mathrm{S}^2, I) \simeq \mathbb{CP}^1$. The latter also coincides with the compact modular curve $X(2)$.

2.4 The hyperbolic metric

The surface $Y(2)$ admits a uniquely-determined complete hyperbolic metric G which is Kähler with respect to its complex structure. This metric was determined explicitly in [25] and studied further in [26, 27]. It is given by (see Figure 1):

$$\mathrm{d}s^2_G = \rho(\zeta,\bar\zeta)^2 |\mathrm{d}\zeta|^2 \quad , \text{ with } \quad \rho(\zeta,\bar\zeta) = \frac{\pi}{8|\zeta(1-\zeta)|} \, \frac{1}{\mathrm{Re}[\mathcal{K}(\zeta)\mathcal{K}(1-\bar\zeta)]} \quad , \tag{2.4}$$

where:

$$\mathcal{K}(\zeta) = \int_0^1 \frac{\mathrm{d}t}{\sqrt{(1-t^2)(1-\zeta t^2)}} = \frac{\pi}{2}\, {}_2F_1\left(\frac{1}{2},\frac{1}{2};1\Big|\zeta\right)$$

is the complete elliptic integral of the first kind, continued analytically to the complex plane with cut along the interval $[1, +\infty)$ of the real axis. The metric (2.4) differs from the restriction to $Y(2)$ of the Euclidean metric of the plane by the conformal factor ρ^2, which has the effect of pushing each of the points $\zeta = 0, 1, \infty$ to infinite distance. As a result, the hyperbolic surface $(Y(2), G)$ looks like a sphere with three infinitely-long cusps. Notice that each cusp has finite hyperbolic area, even though it is infinitely long. In particular, the surface $Y(2)$ has finite hyperbolic area (equal to 2π).

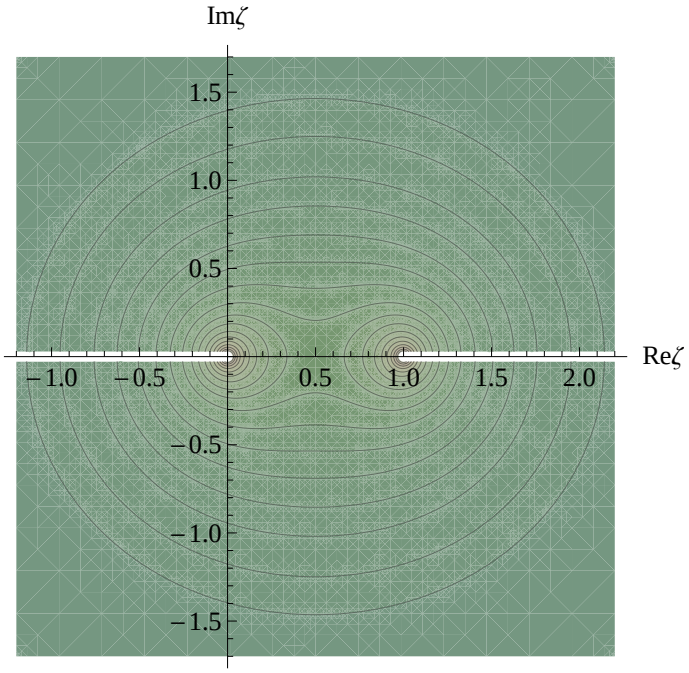

Figure 1: Plot of the hyperbolic density ρ on the twice-punctured plane $Y(2)$. The function $\rho(\zeta, \bar{\zeta})$ grows to infinity at each of the punctures $\zeta = 0, 1$ and tends to zero for $\zeta \to \infty$. The white slots are due to the branch cuts of $\mathcal{K}$, being an artifact produced by the limited numerical precision of the graphics software used.

In principle, the cosmological model can be studied directly on $\mathbb{C} \setminus \{0, 1\}$ using the explicit metric (2.4). However, it is more convenient to lift to $\mathbb{H}$ or to $\mathbb{D}$ as explained in [1] and recalled in Subsection 1.2. Among other advantages, this will allow us to illustrate the effect of projecting through the uniformization map and hence the difference between the behavior of the generalized α-attractor model defined by $Y(2)$ and that of the lifted model defined on the Poincaré half-plane.

2.5 Uniformization to the Poincaré half-plane

The group $\Gamma(2)$. The hyperbolic surface $(Y(2), G)$ is uniformized to the Poincaré half-plane $\mathbb{H}$ with complex coordinate τ (see (0.1)) by the principal congruence subgroup[5] $\Gamma(2) \subset \mathrm{PSL}(2, \mathbb{Z})$, which is defined as the kernel of the surjective group morphism $\mu_2 : \mathrm{PSL}(2, \mathbb{Z}) \to \mathrm{PSL}(2, \mathbb{Z}_2)$ given by:

$$\mu_2\left(\begin{bmatrix} a & b \\ c & d \end{bmatrix}\right) \stackrel{\text{def.}}{=} \begin{bmatrix} a \mod 2 & b \mod 2 \\ c \mod 2 & d \mod 2 \end{bmatrix} \quad .$$

In particular, $\Gamma(2)$ is a normal subgroup of $\mathrm{PSL}(2, \mathbb{Z})$. It consists of all matrices $A = \begin{bmatrix} a & b \\ c & d \end{bmatrix} \in \mathrm{PSL}(2, \mathbb{Z})$ for which a and d are odd and b and c are even. This non-Abelian

[5] Notice that we consider $\Gamma(2)$ as a subgroup of $\mathrm{PSL}(2, \mathbb{Z})$ rather than of $\mathrm{SL}(2, \mathbb{Z})$.

group is freely generated by the two parabolic elements:

$$P_\infty = \begin{bmatrix} 1 & 2 \\ 0 & 1 \end{bmatrix} \quad , \quad P_0 = \begin{bmatrix} 1 & 0 \\ -2 & 1 \end{bmatrix} \tag{2.5}$$

which act as:

$$P_\infty(\tau) = \tau + 2 \quad , \quad P_0(\tau) = \frac{\tau}{1 - 2\tau} \quad .$$

We have $\pi_1(Y(2)) \simeq \Gamma(2)$. Notice that $P_0^{-1} = \begin{bmatrix} 1 & 0 \\ 2 & 1 \end{bmatrix}$ (which acts as $P_0^{-1}(\tau) = \frac{\tau}{2\tau+1}$) and that Γ is also generated by P_0^{-1} and P_∞. It is known[6] that the normalizer of $\Gamma(2)$ inside $\mathrm{PSL}(2,\mathbb{R})$ equals $\mathrm{PSL}(2,\mathbb{Z})$:

$$N(\Gamma(2)) \stackrel{\text{def.}}{=} N_{\mathrm{PSL}(2,\mathbb{R})}(\Gamma(2)) = \mathrm{PSL}(2,\mathbb{Z}) \quad .$$

We also have $N_{\mathrm{PSL}(2,\mathbb{Z})}(\Gamma(2)) = \mathrm{PSL}(2,\mathbb{Z})$, since $\Gamma(2)$ is a normal subgroup of $\mathrm{PSL}(2,\mathbb{Z})$.

The group $\mathrm{PSL}(2,\mathbb{Z}_2)$**.** The group $\mathrm{PSL}(2,\mathbb{Z}_2)$ has six elements, which we denote by:

$$\begin{aligned} a_1 &= \begin{bmatrix} \hat{1} & \hat{0} \\ \hat{0} & \hat{1} \end{bmatrix} \quad , \quad a_2 = \begin{bmatrix} \hat{0} & \hat{1} \\ \hat{1} & \hat{1} \end{bmatrix} \quad , \quad a_3 = \begin{bmatrix} \hat{1} & \hat{1} \\ \hat{1} & \hat{0} \end{bmatrix} \\ a_4 &= \begin{bmatrix} \hat{0} & \hat{1} \\ \hat{1} & \hat{0} \end{bmatrix} \quad , \quad a_5 = \begin{bmatrix} \hat{1} & \hat{1} \\ \hat{0} & \hat{1} \end{bmatrix} \quad , \quad a_6 = \begin{bmatrix} \hat{1} & \hat{0} \\ \hat{1} & \hat{1} \end{bmatrix} \quad . \end{aligned} \tag{2.6}$$

It is isomorphic with the permutation group S_3 on three elements, where a_1, a_2 and a_3 (the last two of which have order 3) correspond to the alternating subgroup A_3 (which for S_3 consists of the cyclic permutations) while a_4, a_5 and a_6 (which have order 2) correspond to the transpositions.

The uniformizing map. The holomorphic covering map $\pi_{\mathbb{H}} : \mathbb{H} \to Y(2)$ is given [15, Chapter 7] by the elliptic modular lambda function $\lambda : \mathbb{H} \to Y(2)$, which is defined through:

$$\lambda(\tau) = \frac{\wp_\tau(\frac{1+\tau}{2}) - \wp_\tau(\frac{\tau}{2})}{\wp_\tau(\frac{1}{2}) - \wp_\tau(\frac{\tau}{2})} \quad ,$$

where:

$$\wp_\tau(z) \stackrel{\text{def.}}{=} \frac{1}{z^2} + \sum_{(m,n)\in\mathbb{Z}^2\setminus\{(0,0)\}} \left(\frac{1}{(z-m-n\tau)^2} - \frac{1}{(m+n\tau)^2} \right)$$

is the Weierstrass elliptic function of modulus τ. The function $\lambda(\tau)$ is invariant under the action of $\Gamma(2)$ on $\mathbb{H}$:

$$\lambda(\frac{a\tau+b}{c\tau+d}) = \lambda(\tau) \quad , \quad \forall A = \begin{bmatrix} a & b \\ c & d \end{bmatrix} \in \Gamma(2)$$

and satisfies:

$$\lambda(\tau+1) = \frac{\lambda(\tau)}{\lambda(\tau)-1} \quad , \quad \lambda(-\frac{1}{\tau}) = 1 - \lambda(\tau) \quad .$$

[6] More generally, the normalizer inside $\mathrm{PSL}(2,\mathbb{R})$ of any principal congruence subgroup $\Gamma(N)$ of $\mathrm{PSL}(2,\mathbb{Z})$ equals $\mathrm{PSL}(2,\mathbb{Z})$. See [28, Corollary 3.6 (vi)]. This statement also follows from [29, Theorem 6].

The anharmonic action of $\mathrm{PSL}(2,\mathbb{Z}_2)$ on $Y(2)$. Given $A \in \mathrm{PSL}(2,\mathbb{Z})$, we have $\lambda(A\tau) = \lambda(\tau)$ for all $\tau \in \mathbb{H}$ iff A belongs to the subgroup $\Gamma(2)$. Hence the orbits of $\Gamma(2)$ on $\mathbb{H}$ consist of the λ-preimages of the points of $Y(2)$. The short exact sequence:

$$1 \to \Gamma(2) \hookrightarrow \mathrm{PSL}(2,\mathbb{Z}) \xrightarrow{\mu_2} \mathrm{PSL}(2,\mathbb{Z}_2)$$

gives the isomorphism of groups:

$$\mathrm{PSL}(2,\mathbb{Z})/\Gamma(2) \simeq \mathrm{PSL}(2,\mathbb{Z}_2) \quad . \tag{2.7}$$

The group $N(\Gamma(2))/\Gamma(2) = \mathrm{PSL}(2,\mathbb{Z})/\Gamma(2)$ acts on the quotient $Y(2) = \mathbb{H}/\Gamma(2)$ as in (1.8). Composing this with the isomorphism (2.7) gives the *anharmonic action* of $\mathrm{PSL}(2,\mathbb{Z}_2)$ on $Y(2)$:

$$a\zeta = \lambda(A\tau) \quad , \quad \forall a = \mu_2(A) \in \mathrm{PSL}(2,\mathbb{Z}_2) \quad \forall \zeta = \lambda(\tau) \in Y(2) \quad ,$$

where $A \in \mathrm{PSL}(2,\mathbb{Z})$ and $\tau \in \mathbb{H}$. A collection of coset representatives for a_j in the quotient $\mathrm{PSL}(2,\mathbb{Z})/\Gamma(2)$ is provided by the following elements of $\mathrm{PSL}(2,\mathbb{Z})$:

$$\begin{aligned} A_1 &= \begin{bmatrix} 1 & 0 \\ 0 & 1 \end{bmatrix} \quad , \quad A_2 = \begin{bmatrix} 0 & 1 \\ -1 & 1 \end{bmatrix} \quad , \quad A_3 = \begin{bmatrix} 1 & -1 \\ 1 & 0 \end{bmatrix} \quad , \\ A_4 &= \begin{bmatrix} 0 & 1 \\ -1 & 0 \end{bmatrix} \quad , \quad A_5 = \begin{bmatrix} 1 & 1 \\ 0 & 1 \end{bmatrix} \quad , \quad A_6 = \begin{bmatrix} 1 & 0 \\ 1 & 1 \end{bmatrix} \quad , \end{aligned} \tag{2.8}$$

which act on $\mathbb{H}$ as follows:

$$\begin{aligned} A_1(\tau) &= \tau \quad , \quad A_2(\tau) = \frac{1}{1-\tau} \quad , \quad A_3(\tau) = \frac{\tau - 1}{\tau} \\ A_4(\tau) &= -\frac{1}{\tau} \quad , \quad A_5(\tau) = \tau + 1 \quad , \quad A_6(\tau) = \frac{\tau}{\tau + 1} \quad . \end{aligned}$$

Notice that A_2, A_3 and A_4 are elliptic, while A_5 and A_6 are parabolic. Using these lifts of a_j, we find that the anharmonic action of $\mathrm{PSL}(2,\mathbb{Z}_2)$ on $Y(2)$ is given by:

$$\begin{aligned} a_1(\zeta) &= \zeta \quad , \quad a_2(\zeta) = \frac{1}{1-\zeta} \quad , \quad a_3(\zeta) = \frac{\zeta - 1}{\zeta} \\ a_4(\zeta) &= 1 - \zeta \quad , \quad a_5(\zeta) = \frac{\zeta}{\zeta - 1} \quad , \quad a_6(\zeta) = \frac{1}{\zeta} \quad , \end{aligned} \tag{2.9}$$

thus coinciding with the restriction to $Y(2)$ of the action on $\mathbb{CP}^1$ of the following elements of the Moebius group $\mathrm{PSL}(2,\mathbb{C})$:

$$\begin{aligned} B_1 &= \begin{bmatrix} 1 & 0 \\ 0 & 1 \end{bmatrix} \quad , \quad B_2 = \begin{bmatrix} 0 & 1 \\ -1 & 1 \end{bmatrix} \quad , \quad B_3 = \begin{bmatrix} 1 & -1 \\ 1 & 0 \end{bmatrix} \quad , \\ B_4 &= \begin{bmatrix} -\mathbf{i} & \mathbf{i} \\ 0 & \mathbf{i} \end{bmatrix} \quad , \quad B_5 = \begin{bmatrix} \mathbf{i} & 0 \\ \mathbf{i} & -\mathbf{i} \end{bmatrix} \quad , \quad B_6 = \begin{bmatrix} 0 & \mathbf{i} \\ \mathbf{i} & 0 \end{bmatrix} \quad . \end{aligned} \tag{2.10}$$

The anharmonic group. The six elements (2.10) form a classical subgroup $\mathfrak{B}$ of $\mathrm{PSL}(2,\mathbb{C})$ known as the *anharmonic group*. The correspondence $a_j \to B_j$ gives an isomorphism of groups between $\mathrm{PSL}(2,\mathbb{Z}_2)$ and $\mathfrak{B}$ showing, in particular, that $\mathfrak{B}$ is isomorphic with the permutation group S_3. The anharmonic group coincides with the group of biholomorphisms of the complex curve $Y(2) = \mathbb{C}\backslash\{0,1,\infty\}$, consisting of those elements of the Moebius group $\mathrm{PSL}(2,\mathbb{C})$ which stabilize the set of punctures $\{0,1,\infty\} \subset \mathbb{CP}^1$. The elements of $\mathfrak{B}$ permute the set of punctures as shown in Table 1 (which in particular gives an explicit isomorphism between $\mathfrak{B}$ and the permutation group S_3).

B_j	0	1	∞
B_1	0	1	∞
B_2	1	∞	0
B_3	∞	0	1
B_4	1	0	∞
B_5	0	∞	1
B_6	∞	1	0

Table 1: Action of the anharmonic group on the punctures $\{0,1,\infty\}$. Each of the punctures is fixed by one of the subgroups $\{1, B_j\}$ (with $j = 4,5,6$), which corresponds to the $\mathbb{Z}_2$ subgroup of S_3 generated by the corresponding transposition.

The elements B_4, B_5 and B_6 respectively fix the points $1/2$, 2 and -1 on $Y(2)$, while each of B_2 and B_3 fixes both of the points $e^{\frac{\mathbf{i}\pi}{3}}$ and $e^{-\frac{\mathbf{i}\pi}{3}}$. On the entire Riemann sphere, the elements B_4, B_5 and B_6 also respectively fix the punctures ∞, 0 and 1 (see Table 2).

Element	B_2	B_3	B_4	B_5	B_6
$Y(2)$	$e^{\pm\frac{\mathbf{i}\pi}{3}}$	$e^{\pm\frac{\mathbf{i}\pi}{3}}$	$1/2$	2	-1
$\mathbb{CP}^1 \setminus Y(2)$	none	none	∞	0	1

Table 2: Fixed points for the action of B_j $(j = 2,\ldots,5)$ on $\mathbb{CP}^1$. For each element, the fixed points lying on $Y(2)$ and those that belong to the set $\{0,1,\infty\}$ of punctures are shown on separate lines.

The points $\{e^{+\frac{\mathbf{i}\pi}{3}}, e^{-\frac{\mathbf{i}\pi}{3}}\}$ form an orbit of $\mathfrak{B}$, as do the points $\{-1, 1/2, 2\}$. The action of $\mathfrak{B}$ on these orbits is given in Tables 3 and 4.

	B_1	B_2	B_3	B_4	B_5	B_6
$e^{\frac{\mathbf{i}\pi}{3}}$	$e^{\frac{\mathbf{i}\pi}{3}}$	$e^{\frac{\mathbf{i}\pi}{3}}$	$e^{\frac{\mathbf{i}\pi}{3}}$	$e^{-\frac{\mathbf{i}\pi}{3}}$	$e^{-\frac{\mathbf{i}\pi}{3}}$	$e^{-\frac{\mathbf{i}\pi}{3}}$
$e^{\frac{-\mathbf{i}\pi}{3}}$	$e^{-\frac{\mathbf{i}\pi}{3}}$	$e^{-\frac{\mathbf{i}\pi}{3}}$	$e^{-\frac{\mathbf{i}\pi}{3}}$	$e^{\frac{\mathbf{i}\pi}{3}}$	$e^{\frac{\mathbf{i}\pi}{3}}$	$e^{\frac{\mathbf{i}\pi}{3}}$

Table 3: Action of $\mathfrak{B}$ on the orbit $\{e^{+\frac{\mathbf{i}\pi}{3}}, e^{-\frac{\mathbf{i}\pi}{3}}\}$. Each point of this orbit is fixed by the subgroup $\{B_1, B_2, B_3\}$ of $\mathfrak{B}$, which corresponds to the alternating subgroup $A_3 \simeq \mathbb{Z}_3$ of S_3.

	B_1	B_2	B_3	B_4	B_5	B_6
-1	-1	$1/2$	2	2	$1/2$	-1
$1/2$	$1/2$	2	-1	$1/2$	-1	2
2	2	-1	$1/2$	-1	2	$1/2$

Table 4: Action of $\mathfrak{B}$ on the orbit $\{-1, 1/2, 2\}$. Each point of this orbit is fixed by one of the subgroups $\{1, B_j\}$ (with $j = 4, 5, 6$), which corresponds to the $\mathbb{Z}_2$ subgroup of S_3 generated by the corresponding transposition.

The anharmonic group coincides with the group of orientation-preserving isometries of the hyperbolic surface $(Y(2), G)$:

$$\mathrm{Iso}^+(Y(2), G) = \mathfrak{B} \simeq \mathrm{PSL}(2, \mathbb{Z}_2) \simeq S_3 \quad .$$

Since $\mathfrak{B} \simeq \mathrm{PSL}(2, \mathbb{Z}_2) \simeq \mathrm{PSL}(2, \mathbb{Z})/\Gamma(2)$, the topological quotient $Y(2)/\mathfrak{B}$ can be identified with the topological quotient $\mathbb{H}/\mathrm{PSL}(2, \mathbb{Z})$.

2.6 Presentation of $Y(2)$ as a branched cover of the complex plane

Let $q : \mathbb{C} \to \overline{\mathbb{C}} = \mathbb{C} \sqcup \{\infty\} \simeq \mathbb{CP}^1$ be the rational function defined through:

$$z = q(\zeta) \stackrel{\text{def.}}{=} 256 \frac{(1 - \zeta + \zeta^2)^3}{\zeta^2 (1 - \zeta)^2} = 256 \frac{(\zeta - e^{\frac{\mathbf{i}\pi}{3}})^3 (\zeta - e^{-\frac{\mathbf{i}\pi}{3}})^3}{\zeta^2 (1 - \zeta)^2} \quad ,$$

which has poles at $\zeta = 0$ and $\zeta = 1$. This extends to a map $\bar{q} : \mathbb{CP}^1 \to \mathbb{CP}^1$ upon setting $\bar{q}(\infty) = \infty$. The map $\bar{q}$ is invariant under the anharmonic action (2.9) of $\mathrm{PSL}(2, \mathbb{Z}_2)$. Its ramification points are $z = 0$, $z = 2^6 3^3 = 1728$ and $z = \infty$ and we have:

- $\bar{q}^{-1}(\{\infty\}) = \{0, 1, \infty\}$, each preimage point having ramification index two
- $q^{-1}(\{0\}) = \{e^{-\frac{\mathbf{i}\pi}{3}}, e^{+\frac{\mathbf{i}\pi}{3}}\}$, each preimage point having ramification index three
- $q^{-1}(\{1728\}) = \{-1, \frac{1}{2}, 2\}$, each preimage point having ramification index two.

These special level sets of $\bar{q}$ coincide with the short orbits of the action of $\mathfrak{B}$ on $X(2)$ shown in Tables 1, 3 and 4. In particular, q presents $Y(2)$ as a degree six branched cover of the complex plane with complex coordinate z, ramified at the points $z = 0$ and $z = 1728$; it is the projection map of the topological quotient $Y(2) \to Y(2)/\mathfrak{B} = \mathbb{C}$.

2.7 Quotients of $Y(2)$ by $\mathfrak{B}$

Klein's j-function $j : \mathbb{H} \to \mathbb{C}$ (which is invariant under the whole classical modular group $\mathrm{PSL}(2,\mathbb{Z})$) is related to the λ function through:

$$j(\tau) = (q \circ \lambda)(\tau) = 256 \frac{(1 - \lambda(\tau) + \lambda(\tau)^2)^3}{\lambda(\tau)^2 (1 - \lambda(\tau))^2} \quad .$$

This function presents $\mathbb{H}$ as an $\infty : 1$ *branched* cover of the complex plane. The preimage $j^{-1}(\{z\})$ of any point $z \in \mathbb{C}$ is a full orbit of the action of $\mathrm{PSL}(2,\mathbb{Z})$ on $\mathbb{H}$. The topological quotient $\mathbb{H}/\mathrm{PSL}(2,\mathbb{Z}) = Y(2)/\mathfrak{B}$ can be identified with the complex plane $\mathbb{C}$ with coordinate z using the j-function.

One can construct a good orbifold whose underlying space is the complex plane by taking the *orbifold* quotient $\mathfrak{M} \stackrel{\text{def.}}{=} \mathbb{H} /\!\!/ \mathrm{PSL}(2,\mathbb{Z}) = Y(2) /\!\!/ \mathfrak{B}$ instead of the topological quotient. This quotient has orbifold points located at $z = 0$ and $z = 1728$, with isotropy groups $\mathbb{Z}_3$ and $\mathbb{Z}_2$ respectively. It has a natural compactification given by the good orbifold $\overline{\mathfrak{M}} \stackrel{\text{def.}}{=} \mathbb{CP}^1 /\!\!/ \mathfrak{B}$, which has a further singular point at $z = \infty$ with isotropy group $\mathbb{Z}_2$.

Remark. The complex plane $\mathbb{C}$ coincides with the coarse moduli space of elliptic curves. The (uncompactified) moduli stack of elliptic curves with one marked point is $\mathcal{M} = \mathbb{H} /\!\!/ \mathrm{SL}(2,\mathbb{Z}) \simeq Y(2) /\!\!/ (\mathrm{C} \times \mathfrak{B})$, where $\mathrm{C} = \{-1, 1\} \simeq \mathbb{Z}_2$ is the center of $\mathrm{SL}(2,\mathbb{Z})$. Thus $\mathfrak{M}$ is an orbifold two-fold cover of $\mathcal{M}$. On the other hand, the non-compact modular curve $Y(2)$ coincides with the coarse moduli space of elliptic curves with level two structure[7]. The (uncompactified) moduli stack of elliptic curves with level two structure is the quotient $\mathcal{M}[2] = Y(2) /\!\!/ \mathrm{C}$, which is a six-fold cover of $\mathcal{M}$.

2.8 The orbifold hyperbolic metric induced on $\mathfrak{M}$

Since $\mathrm{PSL}(2,\mathbb{Z})$ contains elliptic elements (which have fixed points on $\mathbb{H}$), the Poincaré metric $G_{\mathbb{H}}$ does *not* descend through $j = q \circ \lambda$ to an ordinary Riemannian metric on the topological quotient $\mathbb{C} = \mathbb{H}/\mathrm{PSL}(2,\mathbb{Z}) = Y(2)/\mathfrak{B}$ (in fact, $\mathbb{C}$ admits no complete hyperbolic metric which is compatible with its usual complex structure). Equivalently, the hyperbolic metric G of $Y(2)$ does not descend to an ordinary metric on the quotient, because the action of $\mathfrak{B}$ on $Y(2)$ has orbits with non-trivial isotropy.

However, $G_{\mathbb{H}}$ (or G) does descend to a hyperbolic *orbifold* metric on $\mathfrak{M}$. This can be viewed as a metric defined on $\mathbb{C} \setminus \{0, 1728\}$, with conical singularities at $z = 0$ and $z = 1728$. It has the form:

$$\mathrm{d}s_0^2 = \rho_0(z, \bar{z})^2 |\mathrm{d}z|^2$$

where:

$$\rho_0(q(\zeta), \overline{q(\zeta)}) = \frac{\rho(\zeta, \bar{\zeta})}{|q'(\zeta)|} \quad \text{with} \quad q'(\zeta) = \frac{(\zeta+1)(\zeta-2)(2\zeta-1)(1-\zeta+\zeta^2)^2}{\zeta^3(\zeta-1)^3} \quad .$$

Notice that ρ_0 tends to 0 for $z \to \infty$ (i.e. for $\zeta = 0, 1$) and that it tends to $+\infty$ at the orbifold points $z = 0$ and $z = 1728$ (i.e. when $\zeta = e^{\pm \frac{\mathbf{i}\pi}{3}}$ and when $\zeta \in \{-1, 1/2, 2\}$).

[7] Given a natural number $N > 1$, a level N structure on an elliptic curve E defined over the complex numbers is a basis (e_1, e_2) of $H_1(E, \mathbb{Z}_N)$ such that the intersection number $e_1 \cdot e_2 \in \mathbb{Z}_N$ equals $\hat{1} \in \mathbb{Z}_N$. See [30] for an introduction.

2.9 Description of modular-invariant j-models as lifts of generalized α-attractor models

Since the orbifold metric ρ_0 has conical singularities at finite distance, it cannot be used to define an α-attractor model in the sense of [1]. In particular, the $\mathrm{PSL}(2,\mathbb{Z})$-invariant models (the "modular invariant j-models") defined in [8] on the Poincaré half-plane do *not* descend to generalized α-attractor models (in the sense of [1]) defined on the topological quotient $\mathbb{H}/\mathrm{PSL}(2,\mathbb{Z}) = Y(2)/\mathfrak{B} = \mathbb{C}$. However, those models do descend (upon taking the quotient by $\Gamma(2)$ rather than by $\mathrm{PSL}(2,\mathbb{Z})$) to generalized α-attractor models defined on $Y(2)$, whose scalar potential Φ is invariant under the action of the anharmonic group $\mathfrak{B}$. Notice that a generalized α-attractor model defined on $Y(2)$ typically lifts through λ to a model which is invariant only under the action of the subgroup $\Gamma(2)$ rather than under the action of the full classical modular group $\mathrm{PSL}(2,\mathbb{Z})$, since the scalar potential Φ of an α-attractor model with scalar manifold $Y(2)$ need not be invariant under the action of $\mathfrak{B}$. As a consequence, the models of [8] do not provide the most general lift of our $Y(2)$ models to the Poincaré half-plane. To describe the most general lift, one must require invariance of the half-plane model only under $\Gamma(2)$ rather than under $\mathrm{PSL}(2,\mathbb{Z})$.

2.10 A multivalued inverse of λ

A multivalued inverse μ of the holomorphic covering map λ is given as follows in terms of hypergeometric functions:

$$\tau = \mu(\zeta) = \mathbf{i}\frac{{}_2F_1(\frac{1}{2},\frac{1}{2};1|1-\zeta)}{{}_2F_1(\frac{1}{2},\frac{1}{2};1|\zeta)} \quad . \tag{2.11}$$

This multivalued analytic function has monodromy around the punctures $\zeta = 0, 1, \infty$, generated respectively by the transformations P_0, $P_1 \stackrel{\mathrm{def.}}{=} P_\infty P_0$ and P_∞. In particular, a preimage of the point $\zeta = -1$ is given by:

$$\tau_0 = \mathbf{i}\frac{{}_2F_1(\frac{1}{2},\frac{1}{2},1|2)}{{}_2F_1(\frac{1}{2},\frac{1}{2};1|-1)} = 1+\mathbf{i} \quad .$$

2.11 Fundamental polygons

On the Poincaré half-plane. A fundamental polygon for the action of $\Gamma(2)$ on $\mathbb{H}$ is given [15, Sec. 7] by the hyperbolic quadrilateral (see Figure 2a):

$$\mathfrak{D}_{\mathbb{H}} = \{\tau\in\mathbb{H}| -1 < \mathrm{Re}\tau < 0, |\tau+\frac{1}{2}| > \frac{1}{2}\} \cup \{\tau\in\mathbb{H}|0 \le \mathrm{Re}\tau < 1, |\tau-\frac{1}{2}| > \frac{1}{2}\} \quad ,$$

whose ideal vertices are located at the following points on the conformal boundary of the Poincaré half-plane:

$$A : \tau = \infty \ , \ B : \tau = -1 \ , \ C : \tau = 0 \ , \ D : \tau = 1 \quad .$$

The translation $\tau \to \tau + 2$ gives the Poincaré pairing between the sides (AB) and (AD), while the transformation $\tau \to \frac{\tau}{2\tau+1}$ gives the Poincaré pairing between the sides (BC) and (CD), which are the two bounding circle arcs. We have:

$$\lim_{\tau\to\pm 1}\lambda(\tau) = \infty \quad , \quad \lim_{\tau\to 0}\lambda(\tau) = 1 \quad , \quad \lim_{\tau\to\infty}\lambda(\tau) = 0 \quad ,$$

where the limits are taken from within $\mathfrak{D}_{\mathbb{H}}$. The function λ maps the relative frontier of $\mathfrak{D}_{\mathbb{H}}$ onto the region $(-\infty, 0) \cup (1, +\infty)$ of the real axis, taking each of the vertical sides into the interval $(-\infty, 0)$ and each of the two half-circles into the interval $(1, +\infty)$. The vertical half-line which cuts $\mathfrak{D}$ through the middle (and which is part of the y axis) is mapped to the interval $(0, 1)$.

On the hyperbolic disk. The fundamental polygon $\mathfrak{D}_{\mathbb{D}}$ on the hyperbolic disk with complex coordinate u which corresponds to $\mathfrak{D}_{\mathbb{H}}$ through the Cayley transform is the ideal hyperbolic quadrilateral with vertices located at the points (see Figure 2b):

$$A' : u = \mathbf{i} \ , \ B' : u = -1 \ , \ C' : u = -\mathbf{i} \ , \ D' : u = 1 \quad .$$

The diagonals of this quadrilateral are orthogonal to each other. Decomposing $\mathfrak{D}_{\mathbb{D}}$ into ideal triangles gives the hyperbolic area of $Y(2)$:

$$\text{area}(Y(2)) = 2\pi \quad .$$

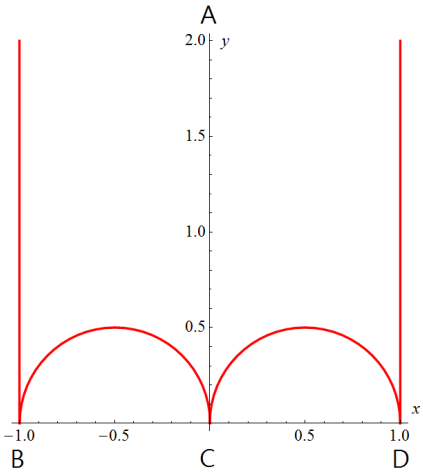

(a) A fundamental polygon $\mathfrak{D}_{\mathbb{H}}$ on the Poincaré half-plane.

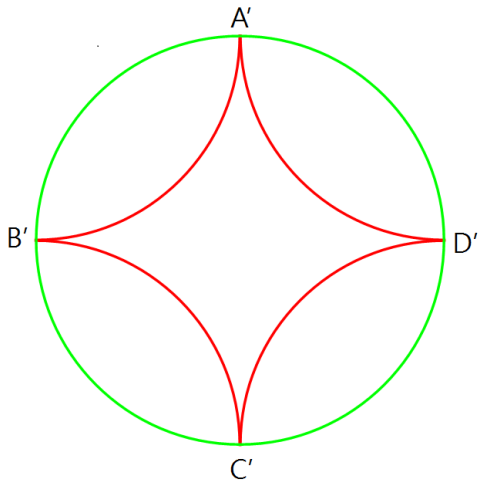

(b) A fundamental polygon $\mathfrak{D}_{\mathbb{D}}$ on the hyperbolic disk.

Figure 2: Fundamental polygons for the uniformization of $Y(2)$ to the Poincaré half-plane and to the hyperbolic disk.

2.12 Local holomorphic cusp coordinates on $Y(2)$

Local holomorphic coordinates u_0, u_1, u_∞ can be constructed around each of the punctures $\zeta = 0, 1, \infty$ as explained in [1, Sec. 5.4]:

1. The point $\tau = \infty$ (which projects to $\zeta = 0$) is invariant under the action of the cyclic subgroup of γ generated by the parabolic element P_∞ of (2.5), which acts as the translation $\tau \to \tau + 2$. The element $T_\infty = \begin{bmatrix} \frac{1}{\sqrt{2}} & 0 \\ 0 & \sqrt{2} \end{bmatrix} \in \text{PSL}(2, \mathbb{R})$ acts as $T_\infty \tau = \frac{\tau}{2}$ and

satisfies $(T_\infty P_\infty T_\infty^{-1})(\tau) = \tau + 1$. Hence the holomorphic cusp coordinate around $\zeta = 0$ is given by [1]:

$$u_0 = e^{2\pi \mathbf{i} T_\infty \tau} = e^{\mathbf{i}\pi\tau} = e^{\pi \mathbf{i} \mu(\zeta)} \quad .$$

In the expression above, it is understood that one chooses a branch of the multivalued inverse (2.11) for which $\tau = \mu(\zeta)$ belongs to the cusp domain:

$$\mathcal{C}_\infty = \{\tau \in \mathbb{H} \,|\, \mathrm{Im}\tau > 2\} \quad .$$

This insures that u_0 covers the punctured disk $0 < |u_0| < e^{-2\pi}$ (see [1, 10]).

2. The point $\tau = 0$ (which projects to $\zeta = 1$) is invariant under the action of the cyclic subgroup of Γ generated by the parabolic element P_0 of (2.5). The element $T_0 = \begin{bmatrix} 0 & \frac{1}{\sqrt{2}} \\ -\sqrt{2} & 0 \end{bmatrix} \in \mathrm{PSL}(2,\mathbb{R})$ acts as $T_0\tau = -\frac{1}{2\tau}$ and satisfies $(T_0 P_\infty T_0^{-1})(\tau) = \tau + 1$. Hence the holomorphic cusp coordinate around $\zeta = 1$ is given by:

$$u_1 = e^{2\pi \mathbf{i} T_0 \tau} = e^{-\frac{\mathbf{i}\pi}{\tau}} = e^{-\frac{\mathbf{i}\pi}{\mu(\zeta)}} \quad .$$

In the expression above, one must choose a branch of μ for which $\tau = \mu(\zeta)$ belongs to the cusp domain:

$$\mathcal{C}_0 = \{\tau \in \mathbb{H} \,|\, \mathrm{Im}\frac{1}{\tau} < -2\} = \{\tau \in \mathbb{H} \,|\, \mathrm{Im}\tau > 2|\tau|^2\} \quad .$$

This insures that u_1 covers the punctured disk $0 < |u_1| < e^{-2\pi}$.

3. The point $\tau = 1$ (which projects to $\zeta = \infty$) is invariant under the action of the cyclic subgroup of Γ generated by the parabolic element:

$$P_1 \stackrel{\mathrm{def.}}{=} P_\infty P_0 = \begin{bmatrix} -3 & 2 \\ -2 & 1 \end{bmatrix} \quad ,$$

which acts as $P_1\tau = \frac{2-3\tau}{1-2\tau}$. The element $T_1 = \begin{bmatrix} 0 & -\frac{1}{\sqrt{2}} \\ \sqrt{2} & -\sqrt{2} \end{bmatrix} \in \mathrm{PSL}(2,\mathbb{R})$ acts as $T_1\tau = \frac{1}{2(1-\tau)}$ and satisfies $(T_1 P_1 T_1^{-1})(\tau) = \tau - 1$. Hence the holomorphic cusp coordinate around $\zeta = \infty$ is given by:

$$u_\infty = e^{2\pi \mathbf{i} T_1 \tau} = e^{\frac{\mathbf{i}\pi}{1-\tau}} = e^{\frac{\mathbf{i}\pi}{1-\mu(\zeta)}} \quad .$$

In the expression above, one must choose a branch of μ for which $\tau = \mu(\zeta)$ belongs to the cusp domain:

$$\mathcal{C}_1 = \{\tau \in \mathbb{H} \,|\, \mathrm{Im}\left(\frac{1}{1-\tau}\right) > 2\} = \{\tau \in \mathbb{H} \,|\, \mathrm{Im}\tau > 2|1-\tau|^2\} \quad .$$

This insures that u_∞ covers the punctured disk $0 < |u_\infty| < e^{-2\pi}$.

Let $c \in \{0, 1, \infty\}$ be any of the punctures, u_c be the local holomorphic cusp coordinate introduced above and $\dot{\mathcal{D}}_c$ be the punctured neighborhood of c in $Y(2)$ defined by $0 < |u_c| < e^{-2\pi}$. The restriction of the hyperbolic metric (2.4) to $\dot{\mathcal{D}}_c$ is given by:

$$\mathrm{d}s^2|_{\dot{\mathcal{D}}_c} = \Lambda(u_c, \bar{u}_c)^2 |\mathrm{d}u_c|^2 \quad , \text{ with } \quad \Lambda(u_c, \bar{u}_c) = \frac{1}{|u_c| \log(1/|u_c|)} \quad . \tag{2.12}$$

This is the standard form of the hyperbolic cusp metric [10, 11]. It can be brought to the form:

$$\mathrm{d}s^2|_{\dot{\mathcal{D}}_c} = \mathrm{d}r^2 + \frac{e^{-2r}}{(2\pi)^2} \mathrm{d}\theta^2 \tag{2.13}$$

upon passing to semi-geodesic coordinates (r_c, θ_c) around the puncture c through the transformation [10]:

$$u_c = e^{2\pi e^{r_c} + \mathbf{i}\theta_c} \quad .$$

In these coordinates, the puncture c is located at $r_c \to +\infty$ and θ runs from 0 to 2π.

3 Cosmological trajectories

In this section, we present numerical examples of cosmological trajectories in generalized α-attractor models defined by $Y(2)$ and in the corresponding lifted models, for certain simple but natural choices of globally well-behaved scalar potentials, with $\alpha = \frac{M_0}{3}$.

3.1 Globally well-behaved scalar potentials on $Y(2)$

Let $\rho = |\zeta|$ and $\theta = \arg(\zeta)$. The embedding (2.3) into the end compactification shows that a smooth potential $\Phi : Y(2) = \mathbb{C} \setminus \{0, 1\} \to \mathbb{R}$ is globally well-behaved iff there exists a smooth map $\hat{\Phi} : X(2) = \mathbb{CP}^1 \simeq \mathrm{S}^2 \to \mathbb{R}$ such that:

$$\Phi(\rho, \theta) = \hat{\Phi}(2 \operatorname{arccot}(\rho), \theta) \quad .$$

Expanding $\hat{\Phi}$ into real (a.k.a. tesseral) spherical harmonics Y_{lm}:

$$\hat{\Phi}(\psi, \theta) = \sum_{l=0}^{\infty} \sum_{m=-l}^{l} D_{lm} Y_{lm}(\psi, \theta)$$

(where D_{lm} are real constants) gives the uniformly-convergent expansion:

$$\Phi(\rho, \theta) = \sum_{l=0}^{\infty} \sum_{m=-l}^{l} D_{lm} Y_{lm}(2 \operatorname{arccot}(\rho), \theta) \quad .$$

Some simple choices for $\hat{\Phi}$ are as follows:

- The following linear combinations of the s (Y_{00}) and p_z (Y_{10}) orbitals:

$$\hat{\Phi}_+(\psi) = M_0 \cos^2\left(\frac{\psi}{2}\right) \quad , \quad \hat{\Phi}_-(\psi) = M_0 \sin^2\left(\frac{\psi}{2}\right) \quad , \tag{3.1}$$

- The following linear combination of the s (Y_{00}) and p_x (Y_{11}) orbitals:

$$\hat{\Phi}_0(\psi,\theta) = M_0(1+\sin\psi\cos\theta) = M_0(1+x_1) \quad . \tag{3.2}$$

- The following linear combination of the s (Y_{00}), d_{z^2} (Y_{20}) and $d_{x^2-y^2}$ (Y_{22}) orbitals:

$$\Phi_1(\psi,\theta) = M_0[1-\sin^2(\psi)\cos^2(\theta)+\cos^2(\psi)] = M_0\left[1-x_1^2+x_3^2\right] \quad .$$

These choices give:

$$\Phi_+ = M_0\frac{\rho^2}{1+\rho^2} \quad , \quad \Phi_- = M_0\frac{1}{1+\rho^2} \quad , \quad \Phi_0 = M_0\left[1+\frac{2\rho\cos\theta}{1+\rho^2}\right]$$
$$\Phi_1 = M_0\left[1-\frac{4\rho^2}{(1+\rho^2)^2}\cos^2\theta+\frac{(1-\rho^2)^2}{(1+\rho^2)^2}\right] \quad . \tag{3.3}$$

Notice that all of these potentials are compactly Morse in the sense of [1]. The extrema of the extended potentials are shown in Table 5.

extremum in coords. (ψ,θ)	$\psi=0$	$\psi=\pi$	$(\psi,\theta)=(\frac{\pi}{2},0)$	$(\psi,\theta)=(\frac{\pi}{2},\pi)$
extremum in coord. ζ	$\zeta=\infty$	$\zeta=0$	$\zeta=1$	$\zeta=-1$
$\hat{\Phi}_+/M_0$	max (1)	min (0)	none (1/2)	none (1/2)
$\hat{\Phi}_-/M_0$	min (0)	max (1)	none (1/2)	none (1/2)
$\hat{\Phi}_0/M_0$	none (1)	none (1)	max (2)	min (0)
$\hat{\Phi}_1/M_0$	max (2)	max (2)	min (0)	min (0)

Table 5: Extrema of extended potentials. In parantheses, we indicate the value of $\hat{\Phi}/M_0$ at the extremum point. Notice that only Φ_0 and Φ_1 have extrema inside $Y(2)$. Also notice that each of the cusp points is an extremum point of $\hat{\Phi}_1$.

Since $\tau_0 = 1+\mathbf{i} \in \mathbb{H}$ is an inverse image of the point $\zeta=-1$, the lifted potentials $\tilde{\Phi}_0$ and $\tilde{\Phi}_1$ have local minima (equal to zero) at the point τ_0 and at each of its images through the action of $\Gamma(2)$. These local minima accumulate toward any point on the conformal boundary $\partial_\infty\mathbb{H}$. The level sets of the potentials $\Phi_\pm$, Φ_0 and Φ_1 and of their lifts to $\mathbb{H}$ are shown in Figures 4, 7, 12 and 16 of the next subsection. Notice that none of these potentials is invariant under the anharmonic group $\mathfrak{B}$.

3.2 Examples of cosmological trajectories

In this subsection, we present four numerically computed trajectories (drawn in black, red, magenta and yellow) for each of the potentials $\Phi_\pm, \Phi_0$ and Φ_1. These trajectories were chosen such that their lifts to $\mathbb{H}$ have the initial conditions at cosmological time $t=0$ shown in Table 6, irrespective of the choice of the scalar potential.

trajectory	τ_0	$\tilde{v}_0$
black	$0.4 + 0.5\mathbf{i}$	$0.3 + \mathbf{i}$
red	$1.4 + 0.5\mathbf{i}$	$0.1 + 0.2\mathbf{i}$
magenta	$0.2 + 0.7\mathbf{i}$	$0.7 + 0.5\mathbf{i}$
yellow	$0.3 + 0.5\mathbf{i}$	0

Table 6: Initial conditions for four trajectories on the Poincaré half-plane.

For each of the four scalar potentials, Table 7 shows which of these initial conditions belong to the inflation region of the corresponding lifted potential. Trajectories which satisfy this condition produce a cosmological scale factor $a(t)$ which is a convex and increasing function of t for some interval starting at $t = 0$. Notice that this condition cannot be satisfied when $\Phi = 0$.

trajectory	Φ_+	Φ_-	Φ_0	Φ_1
black	no	no	no	no
red	yes	no	yes	yes
magenta	no	no	yes	no
yellow	yes	yes	yes	yes

Table 7: Inflationary character of the initial conditions of Table 6 with respect to the scalar potentials $\Phi_\pm$, Φ_0 and Φ_1. The table indicates "yes" when $(\tau_0, \tilde{v}_0)$ belongs to the inflation region of $\tilde{\Phi}$ and "no" otherwise.

Trajectories for $\Phi = 0$. To understand the effect of the hyperbolic geometry, it is instructive to consider first the case when the scalar potential vanishes identically. In this situation, the yellow trajectory (which has vanishing initial speed) remains stationary for all values of the cosmological time, as can be seen by inspecting the system (1.3) and using the Picard-Lindelöf theorem. Any other trajectory on $Y(2)$ ultimately evolves toward one of the cusp points, while its lift to the Poincaré half-plane evolves toward the conformal boundary $\partial_\infty \mathbb{H}$. Hence each cusp point exerts an attractive "effective force". As shown in Figure 3, each projected trajectory spirals in a complicated manner around the cusp points of $Y(2)$, until eventually "falling" deep inside one of the cusp neighborhoods, where it evolves when $t \to +\infty$ toward the corresponding ideal point. In the figures, the initial point of each trajectory is shown as a thick dot.

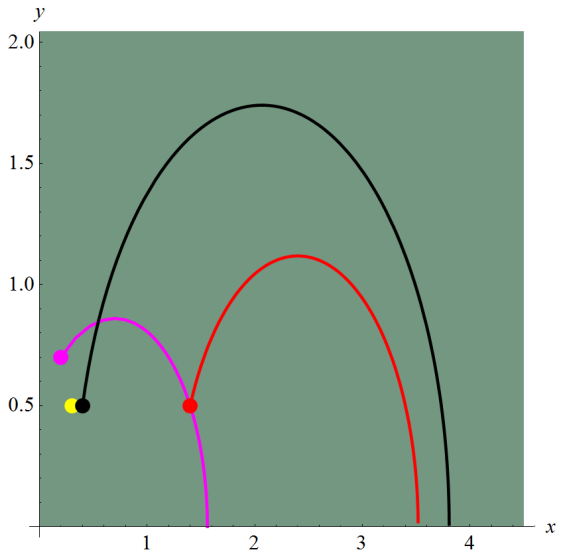

(a) Trajectories for $\tilde{\Phi} = 0$ on the Poincaré half-plane. The solution shown in yellow is stationary.

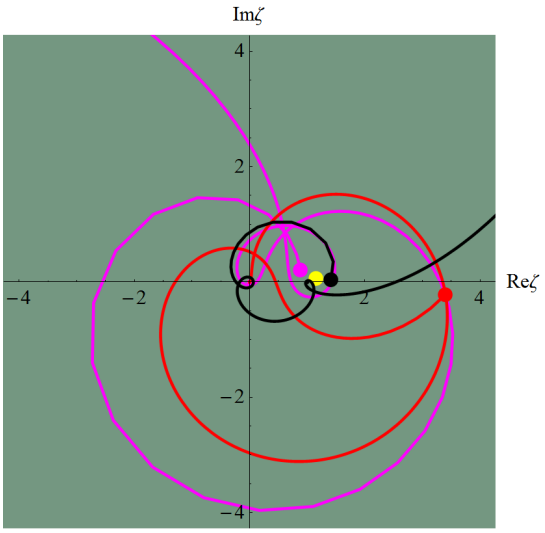

(b) Projection to $Y(2)$ of the trajectories shown at the left.

Figure 3: Numerical solutions for $\Phi = 0$ and $\alpha = \frac{M_0}{3}$.

Trajectories for Φ_+. The level sets of the potential Φ_+ and of its lift $\tilde{\Phi}_+$ to the Poincaré half-plane are shown in Figure 4. This potential has a vanishing infimum at the cusp $\zeta = 0$ and tends to its supremum (which equals M_0) for $\xi \to \infty$.

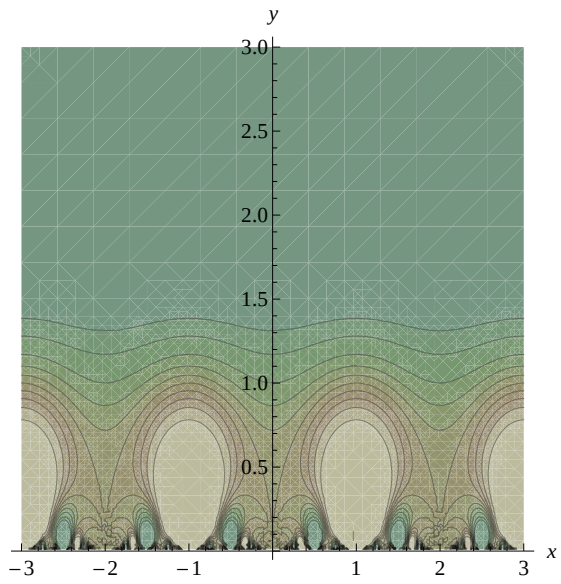

(a) Level plot of $\tilde{\Phi}_+/M_0$ on the Poincaré half-plane.

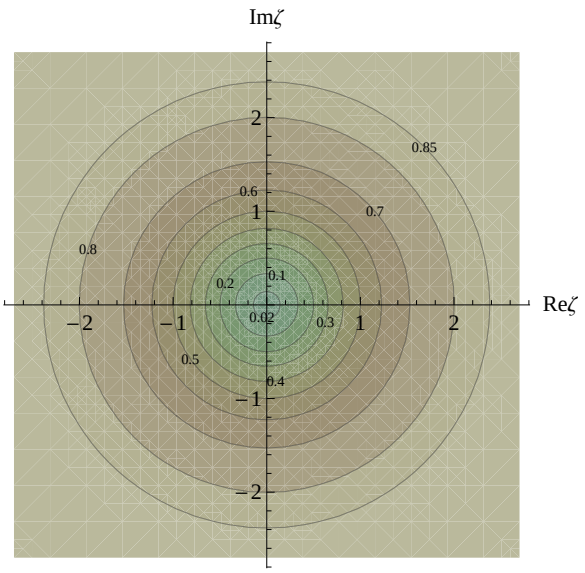

(b) Level plot of Φ_+/M_0 on the twice punctured plane.

Figure 4: Level plots of Φ_+/M_0 and $\tilde{\Phi}_+/M_0$. Darker tones indicate lower values.

The four trajectories whose lifts have the initial conditions given in Table 6 are shown in Figure 5. Due to the effect of the potential, the projected yellow trajectory (which starts with initial velocity zero) evolves toward the cusp point at $\zeta = 0$, as do the other three trajectories. For clarity, Figure 5a shows only a small portion of the trajectories on the Poincaré half-plane.

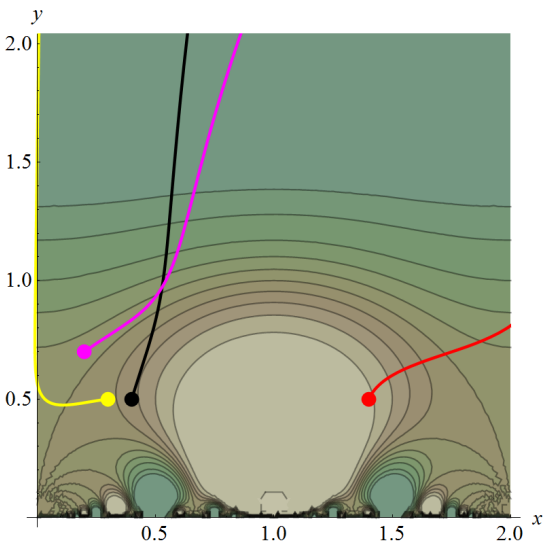

(a) Trajectories for $\tilde{\Phi} = \tilde{\Phi}_+$ on the Poincaré half-plane.

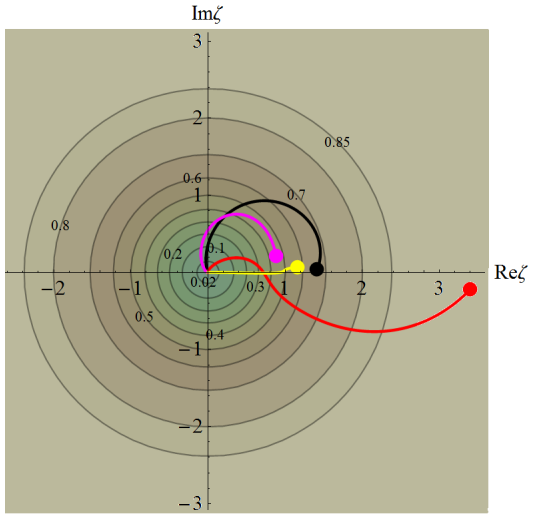

(b) Projection to $Y(2)$ of the trajectories shown at the left.

Figure 5: Numerical solutions for $\Phi = \Phi_+$ and $\alpha = \frac{M_0}{3}$.

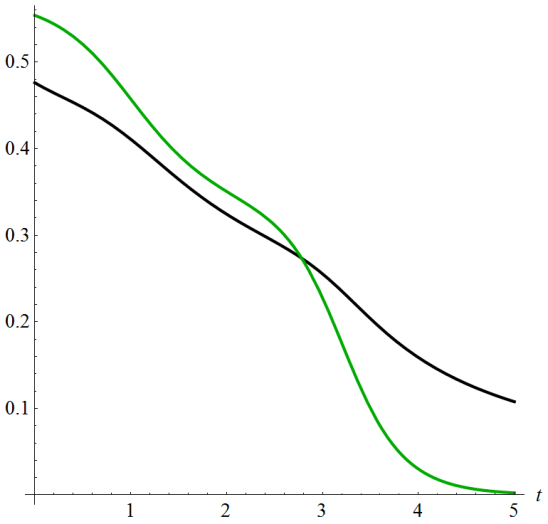

(a) Plot of $H(t)/\sqrt{M_0}$ and $H_c(t)/\sqrt{M_0}$ for the red trajectory.

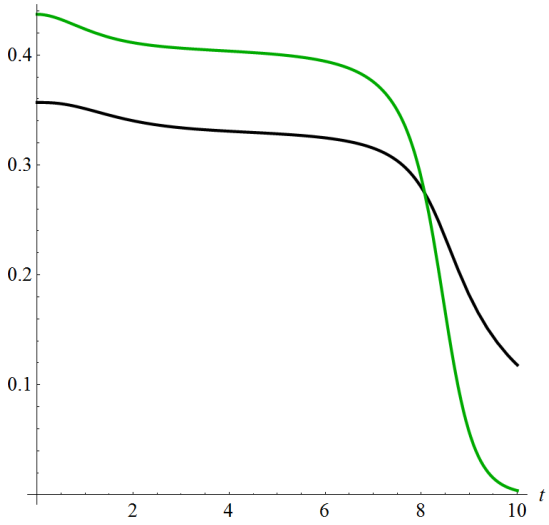

(b) Plot of $H(t)/\sqrt{M_0}$ and $H_c(t)/\sqrt{M_0}$ for the yellow trajectory.

Figure 6: Plot of $H(t)/\sqrt{M_0}$ (black) and $H_c(t)/\sqrt{M_0}$ (green) for the red and yellow trajectories with $\Phi = \Phi_+$ and $\alpha = \frac{M_0}{3}$.

Figure 6 shows the evolution of the Hubble parameter $H(t)$ for the red and yellow trajectories, comparing it with the critical Hubble parameter $H_c(t) \stackrel{\text{def.}}{=} H_c(\varphi(t))$ along that trajectory. As clear from the figure, the tangent vectors of these trajectories lie within the inflation region of Φ_+ for some time interval starting at $t = 0$, thus displaying the behavior expected in inflation.

Trajectories for Φ_-. The level sets of the potential Φ_- and of its lift $\tilde{\Phi}_-$ to the Poincaré half-plane are shown in Figure 7. This potential has a supremum (which equals M_0) at the puncture $\zeta = 0$ and tends to its vanishing infimum for $\zeta \to +\infty$.

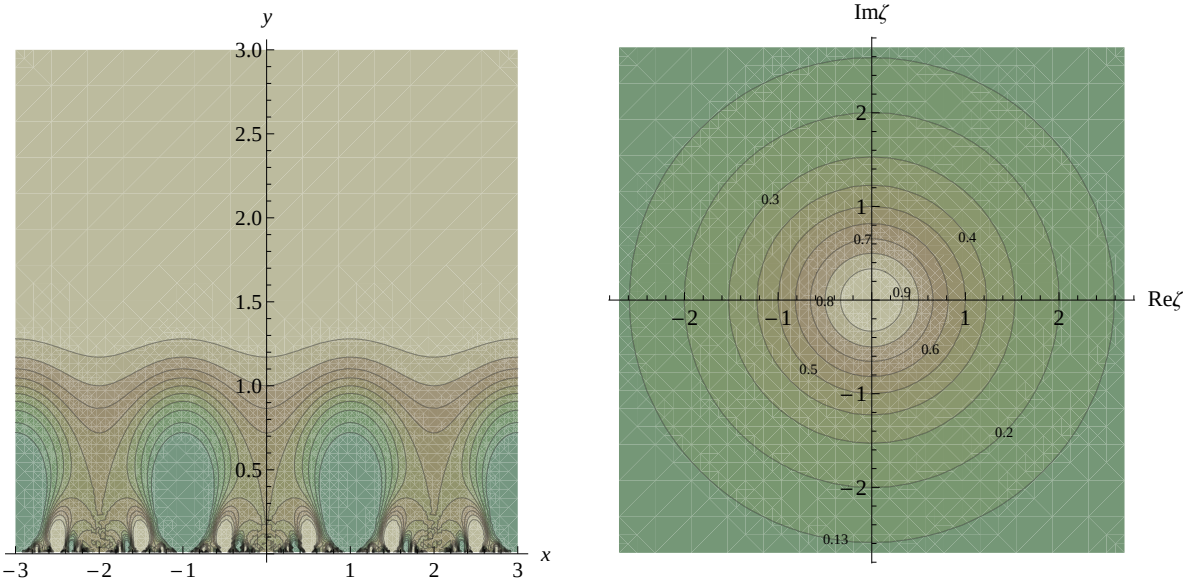

(a) Level plot of $\tilde{\Phi}_-/M_0$ on the Poincaré half-plane.

(b) Level plot of Φ_-/M_- on the twice punctured plane.

Figure 7: Level plots of Φ_-/M_0 and $\tilde{\Phi}_-/M_0$. Darker tones indicate lower values.

Figure 8 shows the lifted trajectories with initial conditions given in Table 6 and their projections through the uniformization map. Despite the repulsive force produced by the potential (which is counterbalanced by the attractive effective force produced by the hyperbolic geometry of the cusp), the yellow trajectory evolves toward the cusp point $\zeta = 0$. As shown in Figure 9, the projected magenta trajectory evolves toward the cusp at infinity, while the projected red trajectory (which, for clarity, is not fully shown in Figure 8b) evolves slowly toward the cusp point at $\zeta = 0$, after winding around it a few times in a complicated manner. The projected black trajectory evolves along a portion of a spiral until it starts heading toward a point close to the real ζ axis and located beyond the cusp at $\zeta = 1$, oscillating around that axis until it seems to stop (see Figure 10). In this example, the repulsive force exerted by the potential is weaker that the effective attraction produced by the cusp at the origin due to the hyperbolic metric.

Figure 11 shows the evolution of the Hubble parameter $H(t)$ along the yellow and black trajectories.

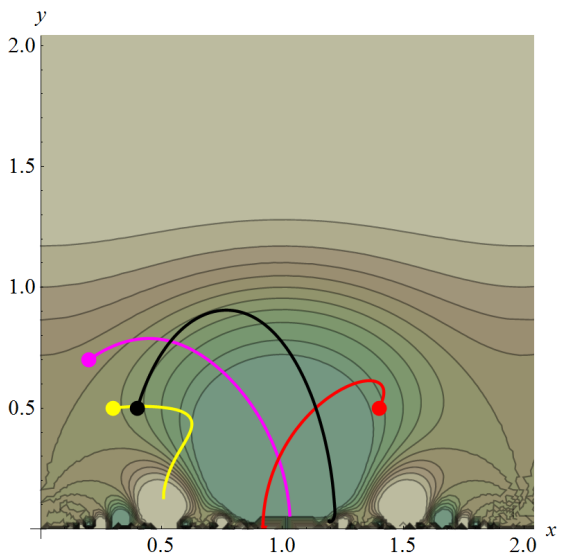

(a) Trajectories for $\tilde{\Phi} = \tilde{\Phi}_-$ on the Poincaré half-plane.

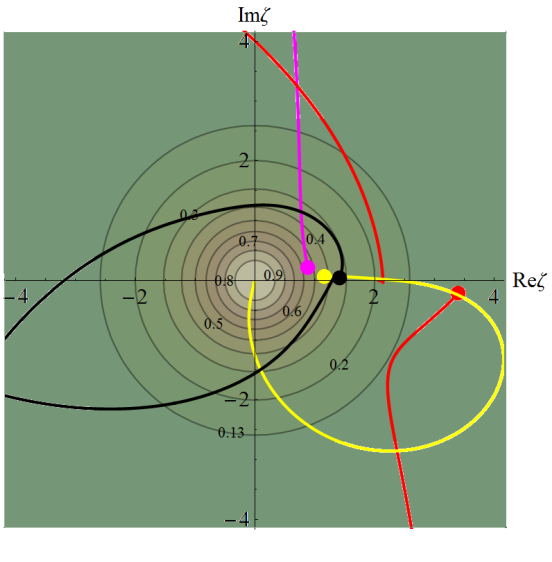

(b) Projection to $Y(2)$ of the trajectories shown at the left. For clarity, we show only the region around the puncture $\zeta = 0$.

Figure 8: Numerical solutions for $\Phi = \Phi_-$ and $\alpha = \frac{M_0}{3}$.

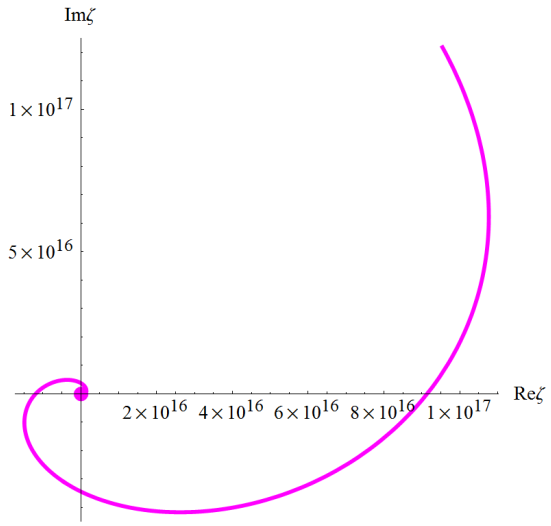

(a) Projected magenta trajectory for the potential Φ_-.

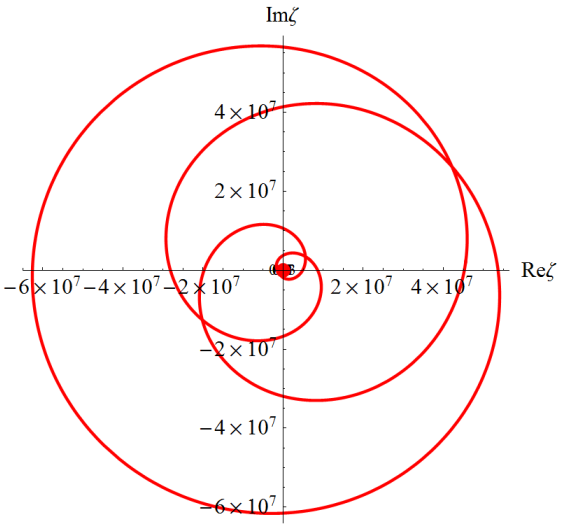

(b) Projected red trajectory for the potential Φ_-.

Figure 9: Large scale view of the red and magenta trajectories for the potential Φ_- with $\alpha = \frac{M_0}{3}$.

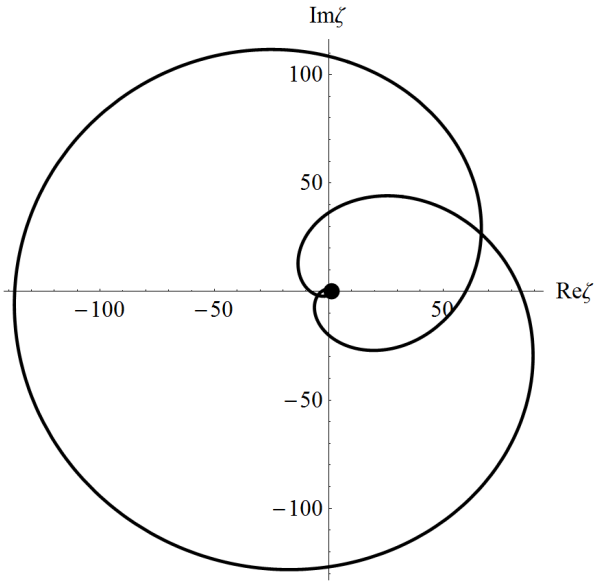

(a) Large scale view of the projected black trajectory for the potential Φ_-

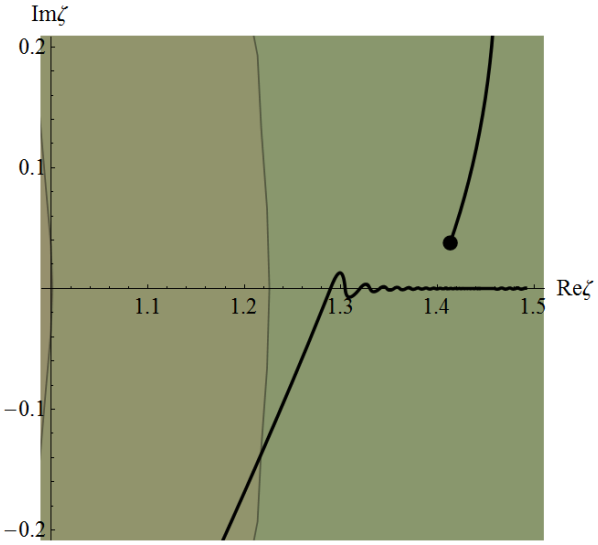

(b) Detail of the beginning and end of the projected black trajectory for the potential Φ_-

Figure 10: The projected black trajectory for the potential Φ_- with $\alpha = \frac{M_0}{3}$.

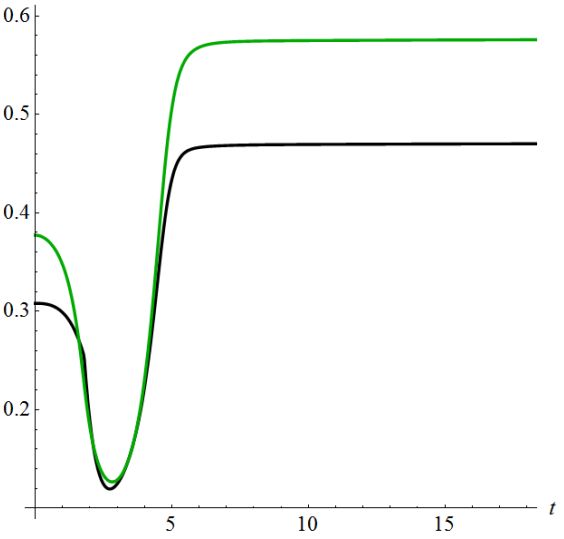

(a) Plot of $H(t)/\sqrt{M_0}$ and $H_c(t)/\sqrt{M_0}$ for the yellow trajectory. This trajectory produces inflation for small t, then exits the inflation regime and re-enters it at some later time.

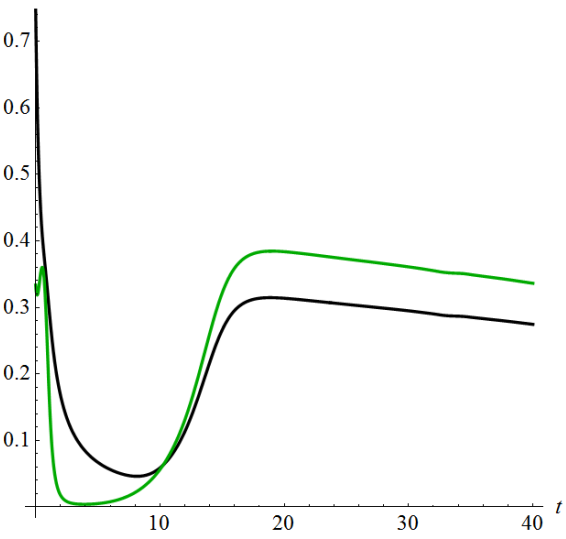

(b) Plot of $H(t)/\sqrt{M_0}$ and $H_c(t)/\sqrt{M_0}$ for the black trajectory. This trajectory does not produce inflation for small t, but it enters the inflation regime at later times.

Figure 11: Plot of $H(t)/\sqrt{M_0}$ (black) and $H_c(t)/\sqrt{M_0}$ (green) for the yellow and black trajectories with $\Phi = \Phi_-$ and $\alpha = \frac{M_0}{3}$.

Trajectories for Φ_0. The level sets of the potential Φ_0 and of its lift $\tilde{\Phi}_0$ to the Poincaré half-plane are shown in Figure 12. This potential has a supremum (which equals $2M_0$) at the cusp $\zeta = 1$ and a vanishing minimum at the point $\zeta = -1$, which lies inside $Y(2)$.

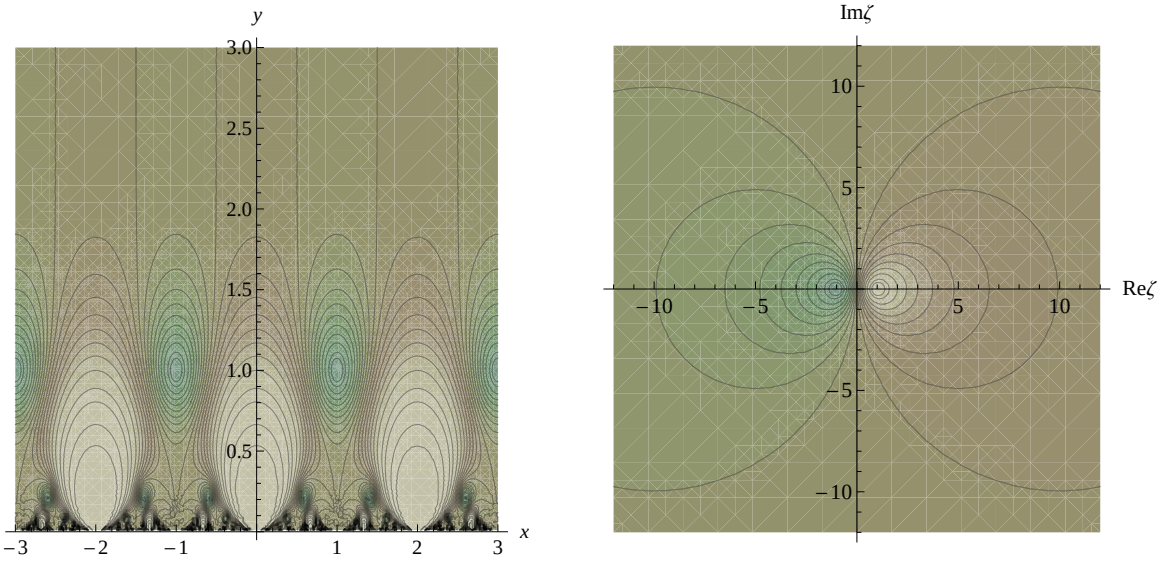

(a) Level plot of $\tilde{\Phi}_0/M_0$ on the Poincaré half-plane.

(b) Level plot of Φ_0/M_0 on the twice punctured plane.

Figure 12: Level plots of Φ_0/M_0 and $\tilde{\Phi}_0/M_0$. Darker tones indicate lower values.

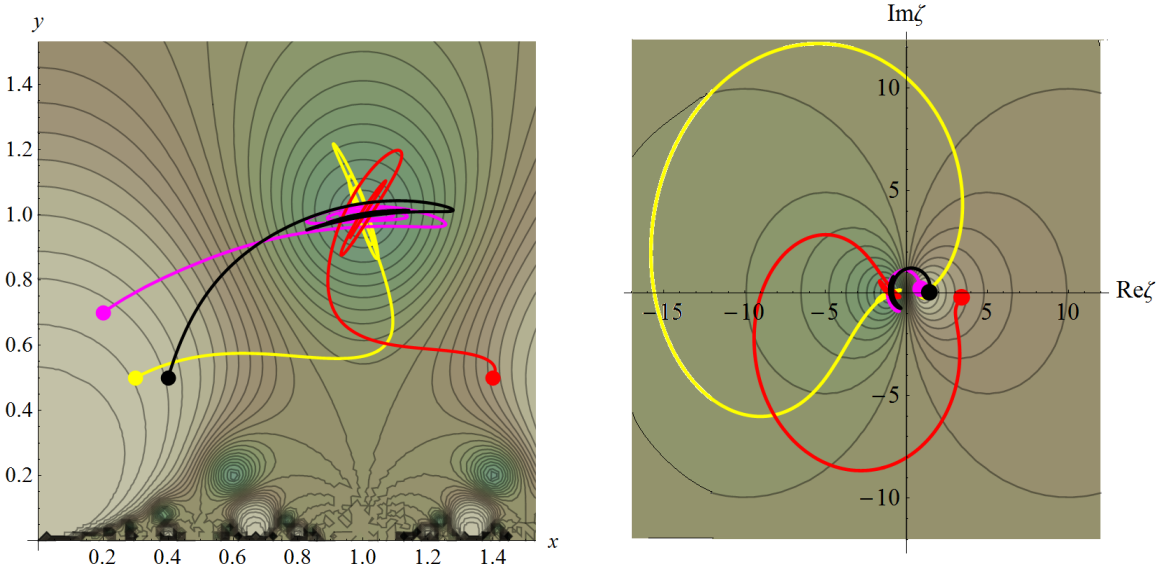

(a) Trajectories for $\tilde{\Phi} = \tilde{\Phi}_0$ on the Poincaré half-plane.

(b) Projection to $Y(2)$ of the trajectories shown at the left.

Figure 13: Numerical solutions for $\Phi = \Phi_0$ and $\alpha = \frac{M_0}{3}$.

Figure 13 shows the four lifted and projected trajectories with initial conditions given in Table 6. All four trajectories eventually evolve toward the minimum point $\zeta = -1$ of Φ_0, after spiraling around it in a complicated manner (see the detail of these trajectories shown in Figure 14). Figure 15 shows the time evolution of the Hubble parameter along the red and magenta trajectories, both of which lead to inflation for some time interval starting at $t = 0$.

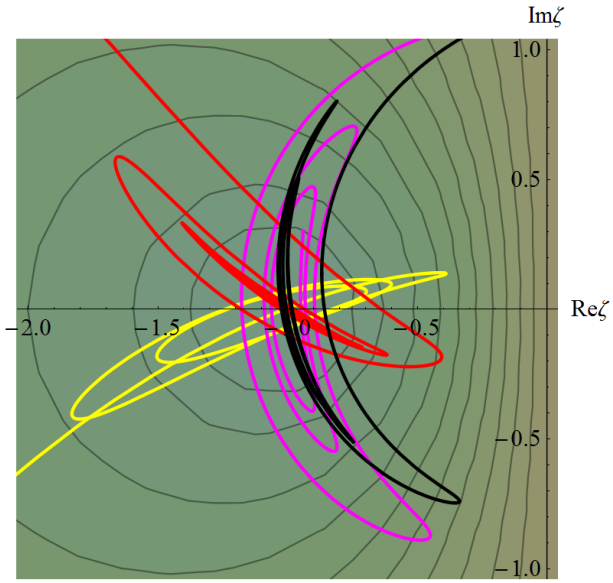

Figure 14: Detail of the projected trajectories close to the minimum of Φ_0, for $\alpha = \frac{M_0}{3}$.

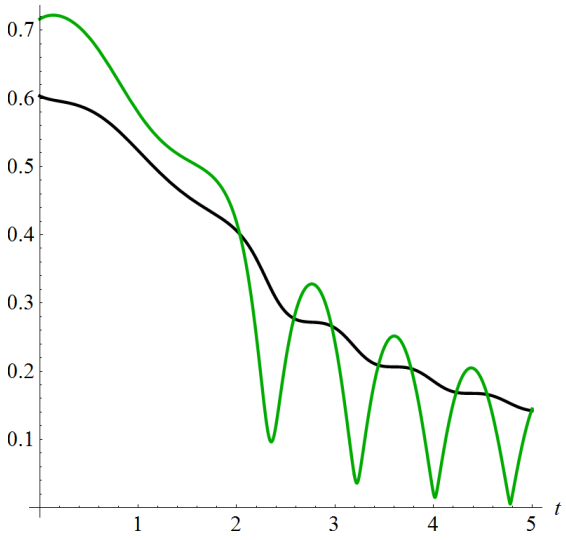

(a) Plot of $H(t)/\sqrt{M_0}$ and $H_c(t)/\sqrt{M_0}$ for the red trajectory.

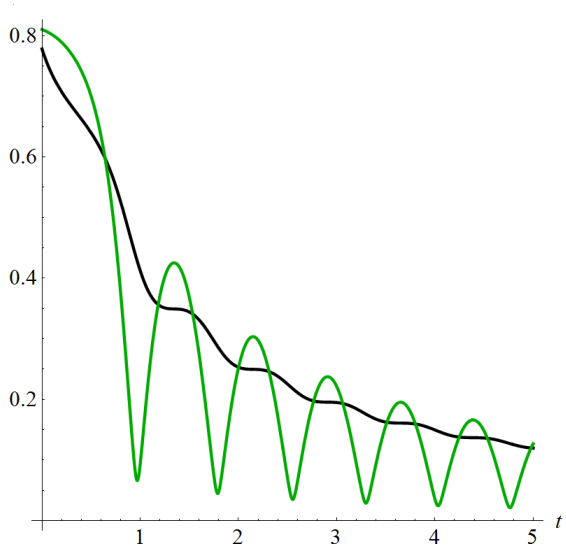

(b) Plot of $H(t)/\sqrt{M_0}$ and $H_c(t)/\sqrt{M_0}$ for the magenta trajectory.

Figure 15: Plot of $H(t)/\sqrt{M_0}$ (black) and $H_c(t)/\sqrt{M_0}$ (green) for the red and magenta trajectories with $\Phi = \Phi_0$ and $\alpha = \frac{M_0}{3}$.

Trajectories for Φ_1. The level sets of the potential Φ_1 and of its lift $\tilde{\Phi}_1$ to the Poincaré half-plane are shown in Figure 16. At the cusp points, this potential tends either to its vanishing infimum (for $\zeta = 1$) or to its supremum, which equals $2M_0$ (for $\zeta = 0, \infty$). Furthermore, it has a minimum (equal to zero) at the point $\zeta = -1$, which lies inside $Y(2)$.

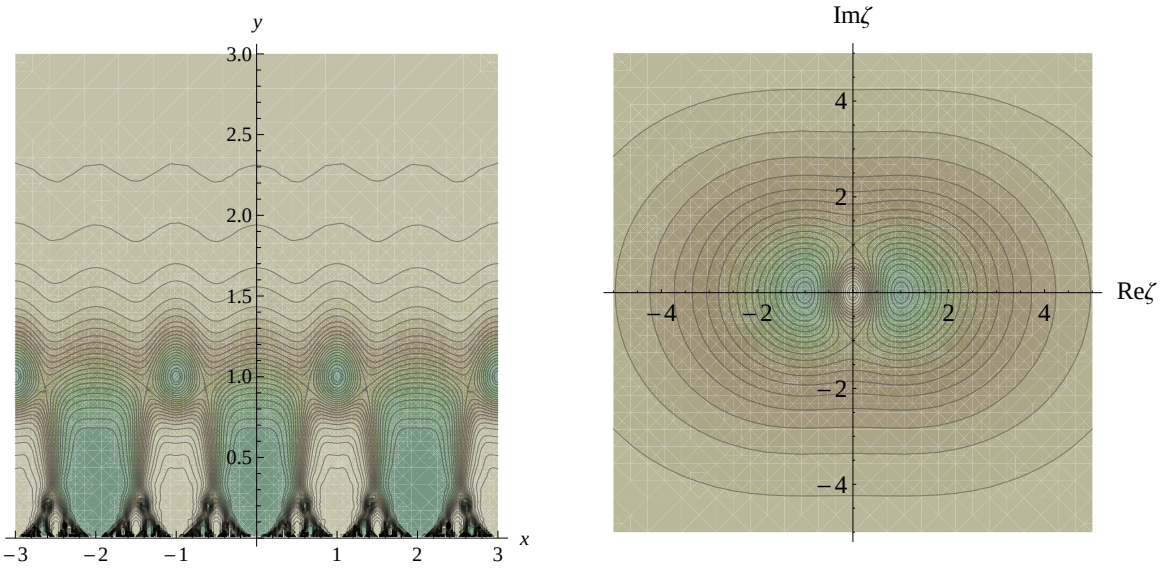

(a) Level plot of $\tilde{\Phi}_1/M_0$ on the Poincaré half-plane.

(b) Level plot of Φ_1/M_0 on the twice punctured plane.

Figure 16: Level plots of Φ_1/M_0 and $\tilde{\Phi}_1/M_0$. Darker tones indicate lower values.

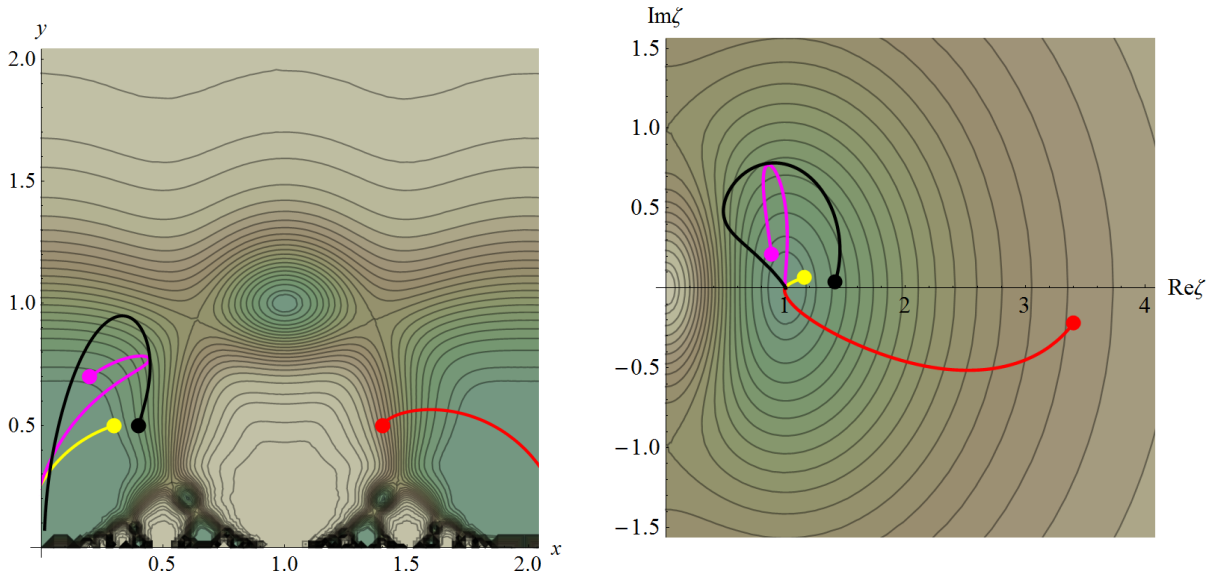

(a) Trajectories for $\tilde{\Phi} = \tilde{\Phi}_1$ on the Poincaré half-plane.

(b) Projection to $Y(2)$ of the trajectories shown at the left.

Figure 17: Numerical solutions for $\Phi = \Phi_1$ and $\alpha = \frac{M_0}{3}$.

The four lifted trajectories with initial conditions given in Table 6 and their projections to $Y(2)$ are shown in Figure 17. All four projected trajectories evolve toward the cusp point $\zeta = 1$, due to the combined effect of the potential (which has an infimum there) and of the effective attractive force produced by the cusp.

Figure 18 shows the time evolution of the Hubble parameter for the red and yellow trajectories, both of which lead to inflation for some (relatively short) cosmological time interval starting at $t = 0$.

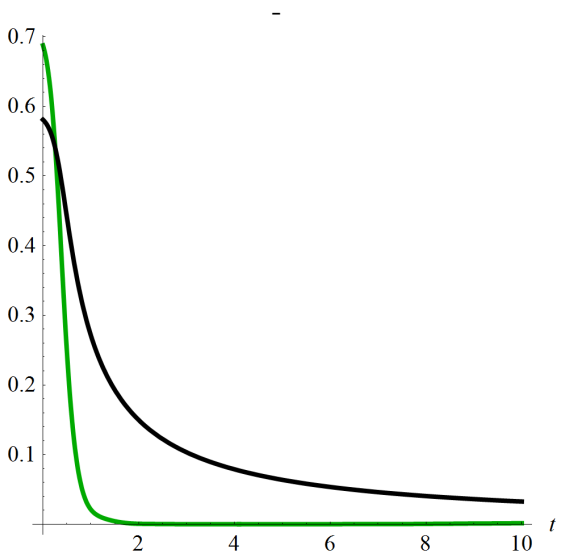

(a) Plot of $H(t)$ and $H_c(t)$ for the red trajectory.

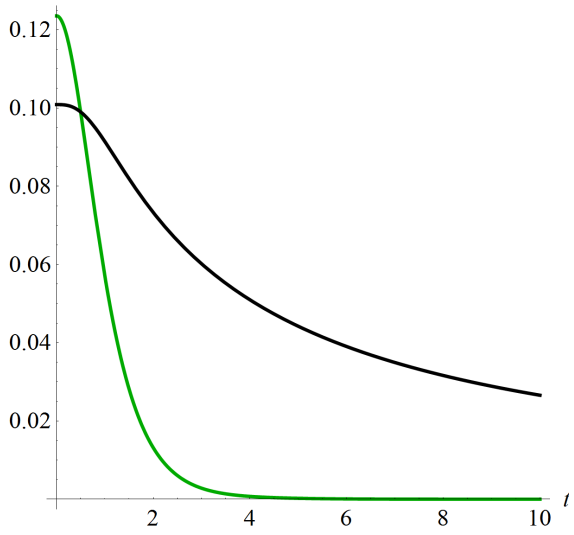

(b) Plot of $H(t)$ and $H_c(t)$ for the yellow trajectory.

Figure 18: Plot of $H(t)/\sqrt{M_0}$ (black) and $H_c(t)/\sqrt{M_0}$ (green) for the red and yellow trajectories with $\Phi = \Phi_1$ at $\alpha = \frac{M_0}{3}$.

4 Conclusions and further directions

We studied cosmological dynamics in generalized α-attractor models defined by the non-compact modular curve $Y(2) = \mathbb{CP}^1 \setminus \{0, 1, \infty\} = \mathbb{C} \setminus \{0, 1\}$, endowed with its unique complete hyperbolic metric. For a few natural choices of globally well-behaved scalar potentials, we computed field trajectories using the methods proposed in [1], finding that the models display intricate behavior. When the scalar potential is invariant under the action of the anharmonic group $\mathfrak{B} \simeq S_3$, we showed that such models provide an equivalent, geometric interpretation of $\mathrm{PSL}(2, \mathbb{Z})$-invariant cosmological models [8], in which the Poincaré half-plane is replaced by the surface $Y(2)$ while the infinite discrete group $\mathrm{PSL}(2, \mathbb{Z})$ is replaced by the finite group $\mathfrak{B}$. The equivalence is induced by the elliptic modular lambda function, which can be viewed as a field redefinition eliminating most of the infinite unphysical ambiguity present in the Poincaré half-plane description.

The present work can be extended in a few directions. For example, it would be interesting to compute cosmological perturbations and observables in generalized α-attractor

models defined by $Y(2)$, for various choices of the scalar potential. Since the SRST approximation in curved field space [32, 33] cannot be applied to most trajectories, such computations could be done numerically using the methods developed in [34–36]. The models discussed in [10] and in this paper could serve as a testing ground for such methods and for probing the corresponding range of phenomenological predictions.

Given any finite index subgroup Γ of $\mathrm{PSL}(2,\mathbb{Z})$, the quotient $Y(\Gamma) = \mathbb{H}/\Gamma$ is called a (non-compact) *modular curve*. When Γ is torsion-free (i.e. contains no elliptic elements), the non-compact hyperbolic surface $Y(\Gamma)$ is geometrically-finite, smooth and has only cusp ends. In particular, $Y(\Gamma)$ has finite area and Γ is a Fuchsian group of the first kind. The classical (but non-generic) case arises when Γ is a congruence subgroup of $\mathrm{PSL}(2,\mathbb{Z})$. All torsion-free congruence subgroups of $\mathrm{PSL}(2,\mathbb{Z})$ whose modular curve has genus zero were classified in reference [31], where it was shown that there exist 33 possibilities up to conjugation inside $\mathrm{PSL}(2,\mathbb{Z})$. The simplest of these is the group $\Gamma(2)$, whose non-compact modular curve $Y(2) \stackrel{\text{def.}}{=} Y(\Gamma(2))$ is the triply-punctured sphere considered in the present paper. For any of the other 32 subgroups, $Y(\Gamma)$ is a sphere with more than 3 punctures. It would be interesting to study generalized α-attractor models defined by these modular curves.

When the scalar potential is preserved by the action of the anharmonic group on $Y(2)$, the generalized α-attractor model has a finite S_3 symmetry. This symmetry cannot be eliminated directly within the framework of [1], since (as explained in Subsection 2.8) taking the Riemannian quotient through the anharmonic group action would lead to a singular hyperbolic metric on the complex plane $\mathbb{C} = Y(2)/\mathfrak{B}$, which cannot be used as a scalar manifold metric in the usual construction of non-linear sigma models. However, it is likely that the definition of non-linear sigma models admits a physically-appropriate generalization to the case when the scalar manifold Σ is replaced by a Riemannian orbifold[8]. It would be interesting to investigate this problem in connection with the larger subject of discrete symmetries of theories coupled to gravity [38], especially in view of applications to string theory compactifications [39, 40].

Finally, it would be interesting to look for embeddings of such models in string theory, perhaps along the lines suggested in [41]. We hope to report on this and related problems in future publications.

Acknowledgments

The work of M.B. and C.I.L. is supported by grant IBS-R003-S1.

References

[1] C. I. Lazaroiu, C. S. Shahbazi, *Generalized α-attractor models from geometrically finite hyperbolic surfaces*, arXiv:1702.06484 [hep-th].

[8] In the context of models with $\mathcal{N} = 1$ supersymmetry, proposals in this direction were made in [37]. Here we are interested in the non-supersymmetric case.

[2] R. Kallosh, A. Linde, D. Roest, *Superconformal Inflationary α-Attractors*, JHEP **11** (2013) 098, arXiv:1311.0472 [hep-th].

[3] R. Kallosh, A. Linde, D. Roest, *Large field inflation and double α-attractors*, JHEP **08** (2014) 052, arXiv:1405.3646 [hep-th].

[4] R. Kallosh, A. Linde, D. Roest, *A universal attractor for inflation at strong coupling*, Phys. Rev. Lett. **112** (2014) 011303, arXiv:1310.3950 [hep-th].

[5] M. Galante, R. Kallosh, A. Linde, D. Roest, *The Unity of Cosmological Attractors*, Phys. Rev. Lett. **114** (2015) 141302, arXiv:1412.3797 [hep-th].

[6] J. J. M. Carrasco, R. Kallosh, A. Linde, D. Roest, *The hyperbolic geometry of cosmological attractors*, Phys. Rev. D **92** (2015) 4, 41301, arXiv:1504.05557 [hep-th].

[7] R. Kallosh, A. Linde, *Escher in the Sky*, Comptes Rendus Physique **16** (2015) 914, arXiv:1503.06785 [hep-th].

[8] R. Schimmrigk, *Modular Inflation Observables and j-Inflation Phenomenology*, arXiv:1612.09559 [hep-th].

[9] H. P. de Saint-Gervais, *Uniformization of Riemann Surfaces: revisiting a hundred-year-old theorem*, EMS, 2016.

[10] M. Babalic, C. I. Lazaroiu, *Generalized α-attractor models from elementary hyperbolic surfaces*, arXiv:1703.01650 [hep-th].

[11] D. Borthwick, *Spectral Theory of Infinite-Area Hyperbolic Surfaces*, Progr. in Math. **256**, Birkhäuser, Boston, 2007.

[12] D. Borthwick, C. Judge, P. A. Perry, *Selberg's zeta function and the spectral geometry of geometrically finite hyperbolic surfaces*, Comment. Math. Helv. **80** (2005) 483–515.

[13] F. Diamond, J. Shurman, *A First Course in Modular Forms*, Graduate Texts in Mathematics, Springer, 2005.

[14] G. Shimura, *Introduction to the Arithmetic Theory of Automorphic Functions*, Princeton U.P., 1971.

[15] L. V. Ahlfors, *Complex analysis* (3rd ed.), Mc. Graw-Hill, 1979.

[16] S. Katok, *Fuchsian Groups*, U. Chicago Press, 1992.

[17] A. F. Beardon, *The geometry of discrete groups*, Graduate Texts in Mathematics **91**, Springer, 1983.

[18] W. Fenchel, J. Nielsen, *Discontinuous Groups of Isometries in the Hyperbolic Plane*, De Gruyter, 2003.

[19] R. Schimmrigk, *Automorphic inflation*, Phys. Lett. B **748** (2015) 376, arXiv: 1412.8537 [hep-th].

[20] R. Schimmrigk, *A geneneral framework of automorphic inflation*, JHEP **05** (2016) 140, arXiv: 1512.09082 [hep-th].

[21] I. Richards, *On the Classification of Non-Compact Surfaces*, Transactions of the AMS **106** (1963) 2, 259–269.

[22] S. Stoilow, *Leçons sur les principes topologiques de la théorie des fonctions analytiques*, Gauthier-Villars, Paris, 1956.

[23] B. Maskit, *Canonical domains on Riemann surfaces*, Proc. Amer. Math. Soc. **106** (1989), 713–721.

[24] A. Haas, *Linearization and mappings onto pseudocircle domains*, Trans. Amer. Math. Soc. **282** (1984), 415–429.

[25] S. Agard, *Distortion theorems for quasiconformal mappings.* Ann. Acad. Sci. Fenn. A I Math. **413** (1968) 1–12.

[26] A . Yu. Solynin, M. Vuorinen, *Estimates for the hyperbolic metric of the punctured plane and applications*, Israeli Journal of Mathematics **124** (2001) 29–60.

[27] T. Sugawa, M. Vuorinen, *Some inequalities for the Poincaré metric of plane domains*, Math. Z. **250** (2005) 4, 885–906.

[28] S. Zemel, *Normalizers of Congruence Groups in $SL_2(\mathbb{R})$ and Automorphisms of Lattices*, arXiv:1512.07547 [math.NT].

[29] M. Newman, *Normalizers of Modular Groups*, Math. Ann. **238** (1978) 2, 123–129.

[30] R. Hain, *Lectures on moduli spaces of elliptic curves*, pp. 95–166 in "Transformation groups and moduli spaces of curves" (eds. L. Ji, S.-T. Yau), Adv. Lectures in Math. **16**, International Press, 2011.

[31] A. Sebbar, *Torsion-free genus zero congruence subgroups of* $\mathrm{PSL}_2(\mathbb{R})$, Duke Math. J. **110** (2001) 2.

[32] C. M. Peterson, M. Tegmark, *Testing Two-Field Inflation*, Phys. Rev. D **83** (2011) 023522, arXiv:1005.4056 [astro-ph.CO].

[33] C. M. Peterson, M. Tegmark, *Non-Gaussianity in Two-Field Inflation*, Phys. Rev. D **84** (2011) 023520, arXiv:1011.6675 [astro-ph.CO].

[34] M. Dias, J. Frazer, D. Seery, *Computing observables in curved multifield models of inflation – A guide (with code) to the transport method*, JCAP **12** (2015) 030, arXiv:1502.03125 [astro-ph.CO].

[35] M. Dias, J. Frazer, D. J. Mulryne, D. Seery, *Numerical evaluation of the bispectrum in multiple field inflation*, JCAP **12** (2016) 033, arXiv:1609.00379 [astro-ph.CO].

[36] D. J. Mulryne, *PyTransport: A Python package for the calculation of inflationary correlation functions*, arXiv:1609.00381 [astro-ph.CO].

[37] S. Hellerman, E. Sharpe, *Sums over topological sectors and quantization of Fayet-Iliopoulos parameters*, Adv. Theor. Math. Phys. **15** (2011) 1141–1199, arXiv:1012.5999 [hep-th].

[38] T. Banks, N. Seiberg *Symmetries and Strings in Field Theory and Gravity*, Phys.Rev. D **83** (2011) 084019, arXiv:1011.5120 [hep-th].

[39] P. G. Camara, L. E. Ibanez, F. Marchesano, *RR photons*, JHEP **09** (2011) 110, arXiv:1106.0060 [hep-th].

[40] M. Berasaluce-Gonzalez, P. G. Camara, F. Marchesano, D. Regalado, A. M. Uranga, *Non-Abelian discrete gauge symmetries in 4d string models*, JHEP **09** (2012) 059, arXiv:1206.2383 [hep-th].

[41] F. Marchesano, G. Shiu, A. M. Uranga, *F-term Axion Monodromy Inflation*, JHEP **09** (2014) 184, arXiv:1404.3040 [hep-th].